



A methodology for feasibility analyses of district heating networks: A case study applied to greenhouse crops

Jerónimo Ramos-Teodoro ^{a,*}, José Domingo Álvarez ^a, José Luis Torres ^b

^a CIESOL-ceiA3, Department of Informatics, University of Almería, La Cañada, 04120, Almería, Spain

^b CIESOL-ceiA3, Department of Engineering, University of Almería, La Cañada, 04120, Almería, Spain

ARTICLE INFO

Keywords:

District heating
Geographic information systems
Cogeneration plant
Graph theory
Minimum Steiner tree
Genetic algorithm

ABSTRACT

In this article, the preliminary routing, sizing, and cost structure of a heat network that supplies energy, in an agrarian district, to greenhouses located around a cogeneration plant in the municipality of El Ejido (Almería) is presented. A genetic algorithm is employed to select a set of points of consumption (plots of land)—which indirectly determine the network routing over the road network—resulting in a project with a better net present value. To obtain the routing, the Steiner tree problem is solved through an approximation that involves several algorithms derived from graph theory and the use of georeferenced information. The design is constrained to ensure technical feasibility, so that the available thermal power from the plant, averaged for hourly periods over a year, is greater than the demand from the greenhouses. The said demand is calculated through an empty-greenhouse climate model, considering temperature setpoints compatible with the most common crops in the region. According to the results, a network of total length equal to 1.3464 km and an average pipe diameter of 0.1532 m would be required to annually supply 8621.4 MWh of heat to 12 points of consumption. The net present value of the project would be 6 417 900 €, considering a 3% discount rate and useful life of 30 years, with an initial investment cost of 1 723 300 € and an annual operation cost of 15 800 € year⁻¹. A sensibility analysis of the variables with greater economic impact is also presented.

1. Introduction

For years, the European Union has been implementing policies for decarbonization in which heat and cold networks are presented as one of the main infrastructures capable of efficiently integrating energy produced from various renewable sources [1]. Although its use is not so widespread globally, its potential as an alternative to meet future heat and cold energy needs has already been demonstrated [2]. The current geopolitical context, in which Europe has recently been hit by an energy crisis [3], suggests that its implementation should be accelerated, as happened in Denmark with the global energy crisis of the 70 s, which is now a pioneer in this type of systems [4].

When it comes to designing a new thermal network, it is very common to use geographic information systems (GIS) to address the spatial aspect with georeferenced information. This is because the location and quantification of production and points of consumption, as well as the pre-existence of roads and buildings that restrict its layout, will determine the total length and, consequently, the investment costs [5]. To cite some examples, the QGIS tool [6] has been used in the feasibility study of a thermal network located in Vitoria-Gasteiz [5], and in the analysis of spatial clusters of points of consumption with potential

for the deployment of this type of networks [7]. Extensions for GIS have also been developed to solve the routing problem automatically, such as the STEFaN algorithm, which can be integrated into QGIS itself [8], or the so-called Comsof Heat [9]. The problem is that they use a pre-established model, hence they lack flexibility when there are specific needs in the design process, if compared to general-purpose tools or programming languages. As for other alternatives, the selection of points of consumption is generally fixed beforehand, even when the optimal routing of the network may mean not guaranteeing supply to all points in that area. Such a problem is not strange, given the fact that “current open-source tools for energy systems simulation and optimization are still relatively limited” [10].

Moreover, the literature available mainly considers cases in urban environments, with commercial or residential buildings, relegating to a second place those networks that could be deployed in industrial or agricultural areas. Whilst the overall energy consumption of the former ones indeed tends to be higher [11], and this may have attracted more attention, one of the factors that indeed determine the economic viability of a thermal network is demand density [12]. Although this factor plays in favor of most urban environments, which

* Corresponding author.

E-mail addresses: jeronimo.rt@ual.es (J. Ramos-Teodoro), jhervas@ual.es (J.D. Álvarez), jltmoreno@ual.es (J.L. Torres).

<https://doi.org/10.1016/j.energy.2024.131695>

Received 30 December 2023; Received in revised form 11 April 2024; Accepted 16 May 2024

Available online 18 May 2024

0360-5442/© 2024 The Author(s). Published by Elsevier Ltd. This is an open access article under the CC BY license (<http://creativecommons.org/licenses/by/4.0/>).

Nomenclature

Symbol	Description (Units)
A	Area of each plot obtained in QGIS (m^2)
\mathbf{A}	Vector of size $N \times 1$ whose elements are the area corresponding to each supply point (m^2)
a	Experimentally adjusted coefficient (slope) to determine the cost of a substation (kW)
b	Experimentally adjusted coefficient (intercept at the origin) to determine the cost of a substation (€)
C_{inv}	Initial network investment costs (€)
C_{op}	Annual network operating costs (€ year ⁻¹)
C_{sub}	Total cost of the substations based on the selected supply points (€)
C_{sub}^j	Substation cost at supply point (j €)
C_1	Experimentally adjusted Persson and Werner coefficient 1 based on country (€ m ⁻¹)
C_2	Experimentally adjusted Persson and Werner coefficient 2 based on country (€ m ⁻²)
c	Cost of the electrical energy that Ence would stop selling in order to operate the thermal supply network (€ kWh ⁻¹)
d_a	Average pipe diameter according to Persson and Werner (m)
$diag()$	Function that returns the vector of its argument in diagonalized form -
E	Energy that would be consumed annually at the selected supply points (kWh year ⁻¹)
e_c	Cover thickness (mm)
$f(HoY)$	Expression that returns the power based on the argument (HoY kW)
G	Global radiation in the horizontal plane (Wm^2)
HoY	Hours elapsed since the beginning of the year (h)
i	Discount rate used to estimate the present value of all cash flows (-)
L	Total network length (m)
$max()$	Function that returns the maximum value of its argument (-)
N	Total number of supply points (-)
n	Number of years corresponding to the useful life of the project (year)
$NPV(x)$	function that returns the current net value of the network as a function of (x €)
P	Perimeter of each plot obtained in QGIS (m)
P_e	Electrical power at the generator terminals (MW)
p	Sales price of the energy consumed (€ kWh ⁻¹)
Q_c	Thermal power generated by the combustion of dry biomass (MW)

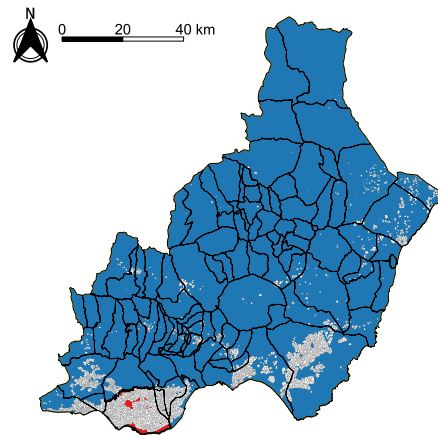


Fig. 1. Contrast view with the location of greenhouses (white), according to SIGPAC data, in El Ejido (red) and in other Almerian municipalities (blue). (For interpretation of the references to color in this figure legend, the reader is referred to the web version of this article.)

energy needs in greenhouses are very diverse, in order to maintain appropriate interior temperature levels for the main activity carried out inside (crop growth), literature shows that annual consumption usually ranges from 3000 MJ m⁻² year⁻¹ in northern European countries to around 150 MJ m⁻² year⁻¹ at latitudes such as those in southeastern Almería [13]. Note that this minimum estimated value for thermal needs in greenhouses (which according to the authors of the study corresponds to an economical strategy, versus optimizing production volume) exceeds by almost an order of magnitude the threshold of 18 MJ m⁻² year⁻¹ considered for the viability of a district heating network.

Finally, Almería is home to the largest concentration of greenhouses in the world, with the greenhouse area of El Ejido being the largest in the province (Fig. 1): 42% of the total, according to 2012 data [14]. Given also the likely future construction of a biomass cogeneration plant in the same area, a project that was initiated in 2017 and has recently obtained environmental authorization from the Junta de Andalucía [15], an opportunity presents itself: these conditions could be compatible with the implementation of a thermal network for greenhouses, as this work aims to determine.

Based on what has been presented so far, the scientific and social interest of this study can be summarized in the following ideas.

- The current design methodologies for heat networks do not consider the selection of favorable or unfavorable points of consumption in the layout. The design is self-limited by including all pre-selected points in the network layout, even when economically it may be more profitable to have a shorter network that only connects those points of consumption with higher demand. In this regard, other authors have highlighted the importance of the initialization strategy adopted for the optimization algorithm [16] and hence a novel technique consisting in pre-determining the layout for a smaller inner ring is also proposed in this study.
- To the best of the authors' knowledge, there are no publications regarding the design of thermal supply networks in agricultural contexts. However, there is interest in greenhouse agriculture in increasing crop production by reproducing favorable climatic conditions, which on many occasions includes injecting CO₂ and/or thermal energy from fossil fuels [14]. There is also interest in analyzing sustainable alternatives to both meet the heat demand due to industrial activities in southeastern Spain [17] and synergistically combine CO₂ capture systems with district heating [18].

usually have multi-story buildings that concentrate demand, some authors consider a minimum threshold value an annual density of 5 GWh km⁻² year⁻¹ [12], which is equivalent to 18 MJ m⁻² year⁻¹. Yet

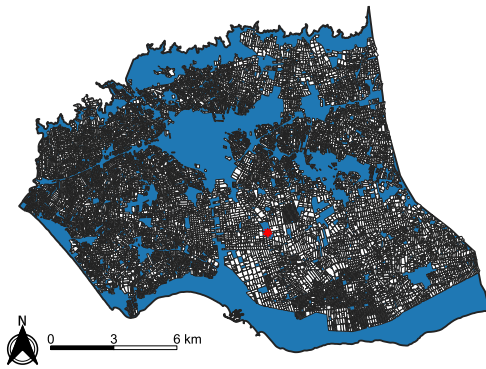


Fig. 2. Contrast view with the location of greenhouses (white), according to SIGPAC data, and the cogeneration plant (red) in the municipality of El Ejido. (For interpretation of the references to color in this figure legend, the reader is referred to the web version of this article.)

- The outcome of this work responds to a potential situation in which useful heat could be wasted at the cogeneration plant. Although, according to the company, that heat is intended to be used in drying the biomass used by the plant, it might happen that at certain times there is more production than heat demand. The existence of a supply network would provide flexibility to the operation of the plant, allowing its distribution to greenhouses when technical or economic reasons so require.

Therefore, the main objective of this work is the predesign and economic analysis of a thermal network to supply a certain number of greenhouses located, as can be seen in Fig. 2, around the plant that Ence Energía y Celulosa, S.A. has projected in El Ejido [15].

2. Materials and methods

The profitability of a heat network is usually analyzed based on investment costs, operational costs, and the benefit obtained from the provision of the supply service, that is, the sale of useful heat [19]. Although a detailed analysis of these would require the complete development of the project, to know the material needs and sizing, it is also possible to carry out a preliminary feasibility analysis based on the tools available in the literature, as detailed in the following sections. A copy of the MATLAB data and code employed in this research study can be found on GitHub¹ and Fig. 3 summarizes the approach adopted with regard to data processing.

As other authors have presented, the available and demanded heats need to be calculated first [20,21], as well as a graph representing all of the possible routes for the pipes of the networks [20].

- To estimate the available heat for the potential consumers, real data from the plant, published by the public administration, has been analyzed and used to define an annual curve, as explained in Section 2.1.
- To estimate the potential demand from the consumers, the typical meteorological year of the region together with a climate model for greenhouses of the municipality have been employed as detailed in Section 2.2.2.
- To locate each possible point of consumption and determine the possible routes for the pipes of the networks public information from the roads and plots of land in the municipality have been processed within QGIS environment to generate a planar graph that has been then exported to MATLAB (see Section 2.2.1).
- A genetic algorithm, fed with the above-said information and executed in MATLAB, is responsible for providing the refined design of the network, as further detailed in Section 2.3.

2.1. Heat availability estimation

In this work, only the costs directly related to the network are analyzed, assuming the existence of thermal energy sources whose construction and operational costs are not part of this analysis (the sale price of thermal energy is). In particular, in this study, only a single heat source is considered, corresponding to the Ence Energía y Celulosa, S.A. cogeneration plant (hereinafter “the plant” or “Ence’s plant”) located in El Ejido. In other words, a monopolistic status with a policy control mechanism based on a price cap, which is the approach for many European countries [22], is assumed.

Since it is necessary to know the thermal generation power or useful heat of the plant, data that has not been disclosed to the media, they can be estimated based on the information available in the Integrated Environmental Authorization (AAI) of the project [23]. On the one hand, Table 1 collects the characteristics of interest for this section according to the design that Ence describes in the AAI. The thermal power of the biomass boiler provided by Ence refers to fuel feed and not to the useful heat of the generated steam, as explained in the AAI itself. Likewise, given the fuel data in Table 1, this fact can be verified, considering the lower heating value (LHV) of biomass (mixed with traces of plastic) and the fuel flow.

On the other hand, according to the main activities required to operate the plant, which are stated in the aforementioned AAI, the heat available for the thermal network (Q_{net}) can be estimated by means of Eq. (1),

$$Q_{net} = \eta_{plant} \cdot Q_c - P_e - Q_{dry} \quad (1)$$

where η_{plant} is the global efficiency of the plant (i.e. considering the thermal power dissipated by any mean, such as gases, ashes, transport processes, electrical generation...), 0.7 according to similar facilities [24] and the International Energy Agency (IEA) reference values [25]; Q_c is the thermal power generated by the combustion of dry biomass, 164.8 MW according to Table 1; P_e is the generated electric power, 40 MW according to Table 1; Q_{dry} is the thermal power required for drying fresh biomass.

To determine Q_{dry} in Eq. (1), several hypotheses were assumed based on the nominal design data for Ence’s plant, as further detailed in Appendix A. As a result, Eq. (2) expresses the considered availability of thermal power for the thermal network (Q_{net}) throughout the year, so that the thermal needs for the drying process can be also met,

$$Q_{net} = \begin{cases} 30\,000 \text{ kW} & \text{From January 1st to April 30th} \\ f(HoY) & \text{From May 1st to June 30th} \\ 0 \text{ kW} & \text{From July 1st to September 30th} \\ 30\,000 \text{ kW} & \text{From October 1st to December 30th} \end{cases} \quad (2)$$

where $f(HoY)$ is an expression that returns the power as a function of the hours elapsed since the beginning of the year (HoY), in a way that it decays, with a constant slope, from 30 000 kW on May 1st to 0 kW on July 1st. Taking into account that the number of hours elapsed, since January 1st, on those two days is 2440 and 3904, respectively, $f(HoY)$ can be defined by Eq. (3).

$$f(HoY) = \frac{-30\,000}{3904 - 2440} \cdot (HoY - 2440) + 3000 \quad (3)$$

2.2. Heat demand estimation

In order to obtain the thermal needs over the year for each possible point of consumption (i.e. a greenhouse), several characteristics, such as type of crop, climatic conditions, and greenhouse area, require to be taken into account. Subsequently, the selection of points of consumption that compose the network is carried out so that the total power does not exceed the value of Q_{net} at any time. This ensures that the needs of consumers are met without excessively compromising the operation of Ence’s plant.

¹ https://github.com/jerort/greenhouses_DHN

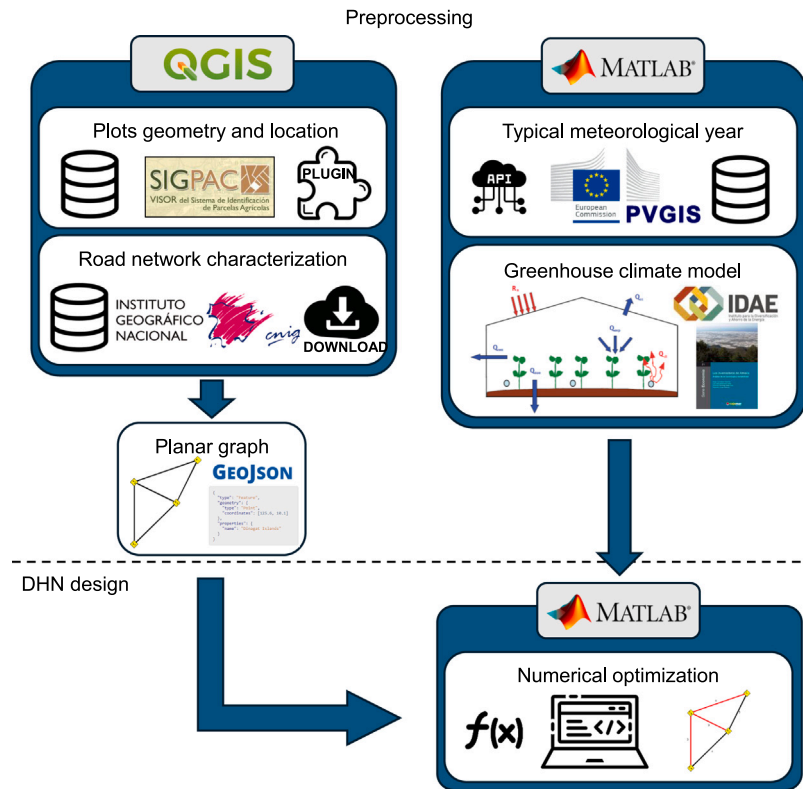


Fig. 3. Schematic overview of the steps required to create the network graph used as an input for the optimization framework.

Table 1
Nominal design data for Ence’s plant.
Source: Retrieved from [23].

Feature	Value
Generated, self-consumed and available electric power	40 MW; 8.5 MW; 31.5 MW
Thermal power of the biomass boiler	164.8 MW
Flow and LHV of the main fuel (vegetable biomass with 25% maximum humidity)	54.4 t/h; 2480 kcal/kg
Mean and maximum percentage of plastic in biomass and LHV of the plastic	1.53%; 3.1%; 9473 kcal/kg
Water sent to the dryer	858.2 t/h; 130 °C
Exhaust gases from the dryer	110 000 m ³ /h; 45 °C

Thus, georeferenced information from the Spanish Geographic Information System of Agricultural Plots, known as SIGPAC [26], can be used, from which the geometry and geographic coordinates of all plots corresponding to greenhouses can be identified. Likewise, the thermal demand curve corresponding to each plot is determined from the climatic data of the region and from established climatic models for greenhouses, on which some simplifications are made [27,28].

2.2.1. Georeferenced points of supply

To work with georeferenced information, QGIS software, a free and open-source geographic information system compatible with multiple platforms [6], is used together with a complement to download SIGPAC’s data [29]. Through these, the enclosures and their respective attributes corresponding to plots in El Ejido (in .gpkg format) are obtained. In addition, since the routing of the network is carried out through roads to save costs, two .shp files from the Spanish National Geographic Institute, known as IGN [30], are used: One corresponds to the transportation networks in the province of Almería and the other to the borders, municipalities, and administrative units. All of the information is related to the ETRS89 reference system [31], in geographic coordinates (EPSG 4258), hence new vector layers with .gpkg extension and reprojected in UTM coordinates (EPSG 25830) are first generated. Because UTM coordinates are expressed in meters, subsequent calculations for the length of the network are facilitated.

The content of the original layers needs to be adapted to generate a graph, whose use is justified in Section 2.3, with all potential points of consumption connected through the road network. First, the road layer from IGN is processed to eliminate undesirable geometries and yield a new layer of linear entities in which all its elements are interconnected, without any isolated road sections. Second, the plots corresponding to greenhouses are identified and processed, eliminating undesirable geometries such as internal rings in polygons, and polygons whose area does not exceed 1000 m² or whose area/perimeter ratio is less than 5 m, leaving a total of 14 746 plots as potential points of consumption (Fig. 4).

Given the constraints on the network design (the routing is limited to the roads present in the processed vector layer), the application of graph theory is very useful [32], as other authors have already pointed out [5,7]. Section 2.3 explains that the layout of the network is determined by a subgraph of the graph corresponding to the entire road network of El Ejido and the possible points of production and supply. The information to construct that graph has been generated in QGIS, as detailed below.

Whilst the points of supply are determined by the location of the greenhouses, the centroid of the plant is approximately located on the satellite view (see Fig. 4 and Fig. 5(a)) at the spot where the boiler would be located, according to the AAI [23]. Its UTM coordinates (ETRS89 30N) are as follows: 520 055.76 E; 4 065 150.53 N. The said

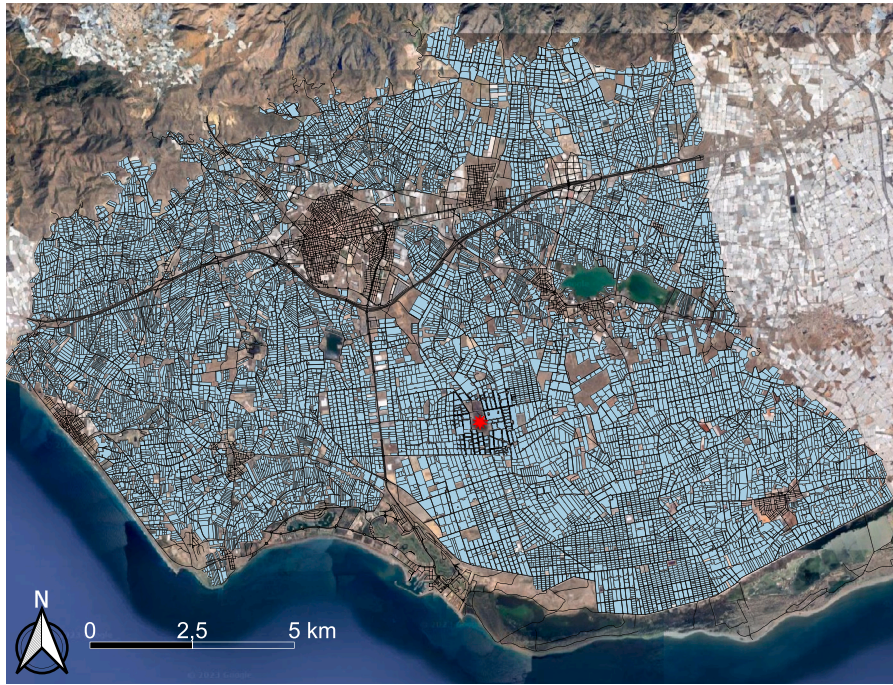


Fig. 4. Vector layers with the roads and greenhouses in El Ejido from which the points and edges of the graph are generated.

centroid together with the centroids of each greenhouse are used to generate, with the help of QGIS's Networks plugin [33], six files (three for EPSG 4258 and three for EPSG 25830) that are exported to MATLAB programming environment [34] in .geojson format, whose content of interest is described below.

- **Connections.** Includes the area and perimeter of each greenhouse and the identifier of the “point of supply”, node to which each greenhouse is connected. A point of supply is defined as a point belonging to a road that is located as close as possible to the centroid of the plot (Fig. 5(a)). A node of this type can supply just one or several greenhouses. The connection segment between the centroid and the point of supply is not part of the network or the graph.
- **Nodes.** Contains the identifier (numeric) of each of the 21 233 nodes of the graph representing the entire road network of El Ejido and the possible points of production and supply (Fig. 5(b)). Each node is assigned two logical attributes to determine whether it is a point of supply and/or production (Ence's plant) or simply a vertex of the road network.
- **Edges.** Contains the identifier of the origin and destination nodes that join each of the 24 384 edges of the graph and their weights, determined by the distance between those two nodes. The distance is calculated with an ellipsoidal projection based on ellipsoid EPSG 7030 [35] and performing a correction based on non-ellipsoidal geometry to consider the elevation of each vertex.

2.2.2. Heating needs in greenhouses

Instead of trying to characterize all the plots of land that have been identified as greenhouses to obtain their potential thermal demand, a single climatic, greenhouse, and crop model is chosen, considering the representative data of the area in which the district heating network would be deployed. In other words, the same thermal demand model for a greenhouse with a geographical reference equal to Ence's plant centroid (36.7315° N; -2.7746° E) is used to simulate and obtain a single annual thermal demand curve per unit area. In combination with the area of each point of consumption, the hourly thermal demand of each plot of land can be obtained. Among the hypotheses considered to justify this decision, it is worth mentioning the following.

- PVGIS, which is used to extract the typical meteorological year of the region, has a geographical resolution of 0.28° [36,37], a value greater than the geographical extension of the plots (0.13° N-S and 0.24° E-W).
- By having a single annual power curve dependent on the area (as opposed to a curve for each plot), the computational burden of the optimization algorithm used for network design (explained in Section 2.3) is reduced.
- It is not possible to determine the state of the crop and, consequently, its transpiration value, without adding a greater (unnecessary) number of assumptions regarding the annual operation of the greenhouses (irrigation, number and type of campaigns, etc.).
- Latent heat due to transpiration tends to be insignificant compared to the rest of the thermal needs when it comes to heating (which is relevant for this study) as opposed to cooling (which is not), as shown, for example, in the practical cases of IDAE's guide [27].
- Air exchange is not necessary due to the absence of crops and the lack of cooling requirements in this study, hence only infiltration losses are considered. An air exchange rate of 2 h⁻¹ is assumed, the minimum value for plastic covers in greenhouses of a certain age [27], since the average greenhouse age is 14 years [14]. This also imposes more restrictive design conditions for the network, as it decreases the energy density of the plots.

To generate the demand curve, the guide of the Institute for Diversification and Energy Saving [27] proposes the energy balance defined by Eq. (4):

$$R_n + Q_{cli} = Q_{cc} + Q_{ren} + Q_{evp} + Q_{soil} \quad (4)$$

where R_n is the net radiation, Q_{cli} is the heat energy supplied/subtracted by the heating/cooling system (depending on the needs), Q_{cc} is the heat lost by conduction and convection through the greenhouse enclosure, Q_{ren} is the sensible and latent heat lost by air renovations and infiltrations, Q_{evp} is the latent heat consumed in the evapotranspiration of plants and soil, Q_{soil} is the heat lost by conduction through the soil. IDAE's guide presents the necessary expressions to determine Q_{cli} from the rest of the variables involved in Eq. (4) [27].

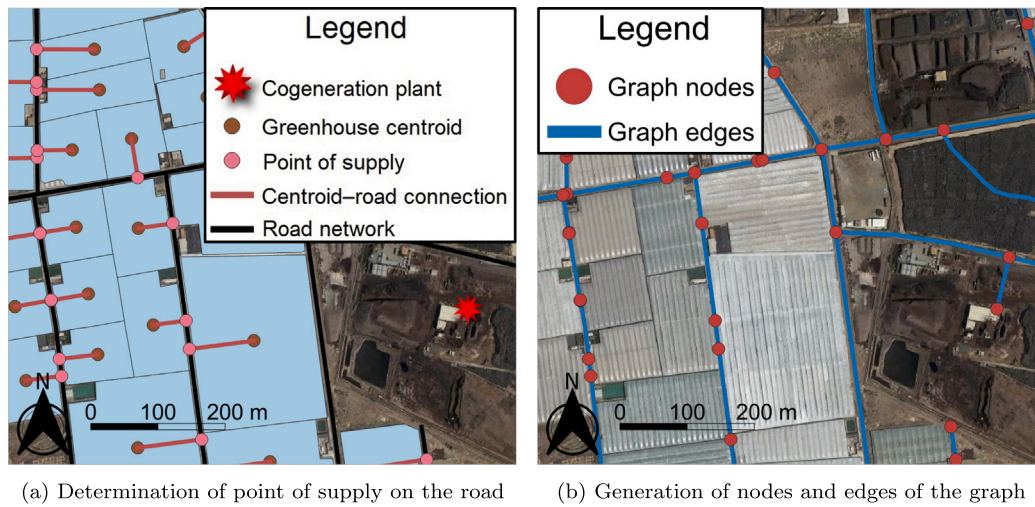


Fig. 5. Data processing in QGIS to be exported in .geojson format to MATLAB.

Table 2

Construction and operational parameters of the greenhouse thermal demand model.

Description	Symbol [27]	Value
Roof absorption coefficient for solar radiation	α	0.04
Soil absorption coefficient for solar radiation	α_s	0.18
Transmission coefficient of the roof for solar radiation	τ	0.89
Cover thermal conductivity	λ_c	$0.33 \text{ Wm}^{-1}\text{C}^{-1}$
Cover thickness	e_c	0.2 mm
Greenhouse air renewal rate	R	2 h^{-1}
Daytime temperature inside the greenhouse	t_i	$22 \text{ }^\circ\text{C}$
Night temperature inside the greenhouse	t_{in}	$10 \text{ }^\circ\text{C}$
Relative humidity inside the greenhouse	–	60%

Neglecting the radiation emitted by the cover, which other authors also do not consider [28], the expression for calculating the net radiation of IDAE’s guide can be rewritten as in Eq. (5), with one term for the radiation absorbed by the ground and another for the greenhouse cover,

$$R_n = G \cdot \alpha \cdot S_d + G \cdot \tau \cdot \alpha_s \cdot S_c \quad (5)$$

where G is the global radiation on the horizontal plane (in W/m^2), α is the absorption coefficient of the cover for solar radiation, S_d is the surface of the greenhouse cover (in m^2), τ is the transmission coefficient of the cover for solar radiation, α_s is the absorption coefficient of the ground for solar radiation, S_c is the surface of the greenhouse ground (in m^2). Given the usual crops and construction parameters in the region [14], a triple-layer coextrusion PE-EVA-PE cover material with a thickness of 800 gauges (0.2 mm) and dry sand soil are considered to determine the parameters shown in Table 2.

As for obtaining the rest of the terms in Eq. (4), considering the parameters shown in Table 2, the expressions shown in IDAE’s guide are strictly used to calculate Q_{cc} and Q_{ren} . The surface convection coefficient for the interior environment of the greenhouse takes a constant value of $7.2 \text{ Wm}^{-1}\text{C}^{-1}$ [38], whereas for the exterior this can be calculated using the equation proposed by the same authors [38]. The characteristics of the PE-EVA-PE cover of 0.2 mm, thickness, and thermal conductivity (Table 2), are also considered. Air losses are considered to occur only due to infiltrations (no ventilation) with a renovation rate of 2 h^{-1} . For the pressure inside the greenhouse, which can be considered equal to atmospheric pressure, typical meteorological year data for the region are used. Also, the contribution of Q_{evp} to Eq. (4) is neglected and to calculate Q_{soil} by means of Eq. (6), it is assumed that, of the total heat losses, “around 10% occur through the soil” [27].

$$Q_{soil} = 0.1 \cdot (Q_{cc} + Q_{ren})/0.9 \quad (6)$$

Given the usual construction parameters in the region [14], greenhouses can be represented as prismatic volumes of high 2.5 m. Eqs. (7) to (9) are used to calculate surfaces and volumes:

$$S_d = 2.5 \cdot P + A \quad (7)$$

$$S_c = A \quad (8)$$

$$V_{gre} = 2.5 \cdot A \quad (9)$$

where P is the perimeter (in m) of the plot obtained by means of QGIS, as explained in 2.2.1, A is the area (in m^2) of the plot obtained by means of QGIS, as explained in 2.2.1, V_{gre} is the volume of air inside the greenhouse (in m^3).

In addition to the parameters mentioned so far, which are constant or a function of each plot, a typical meteorological year or (TMY) corresponding to the geographical coordinates of the centroid of Ence’s plant (36.7315° N ; -2.7746° E) is used. This data set is obtained from the PVGIS platform [36,37] and contains the hourly value of the following meteorological variables for the aforementioned geographical point during an annual period: global radiation on the horizontal plane (in W/m^2), ambient temperature (in $^\circ\text{C}$), relative humidity (in %), wind speed (in m/s), and atmospheric pressure (in Pa). From all of the above, the thermal demand curve for each plot can be obtained, considering only positive values for Q_{cli} .

If the annual energy density of each plot is calculated, by adding up the thermal demand curve over the entire annual period and dividing by the area of the plot, it is possible to obtain the histogram shown in Fig. 6(a). This histogram shows that the 14 746 plots have a very similar energy density according to the applied model, with an average density of $179.11 \text{ MJ m}^{-2} \text{ year}^{-1}$ and a range between $178.41 \text{ MJ m}^{-2} \text{ year}^{-1}$ and $181.51 \text{ MJ m}^{-2} \text{ year}^{-1}$, values consistent with others reported in the literature [13]. For this reason, only the average power curve per unit area of all plots is considered (Fig. 6(b)).

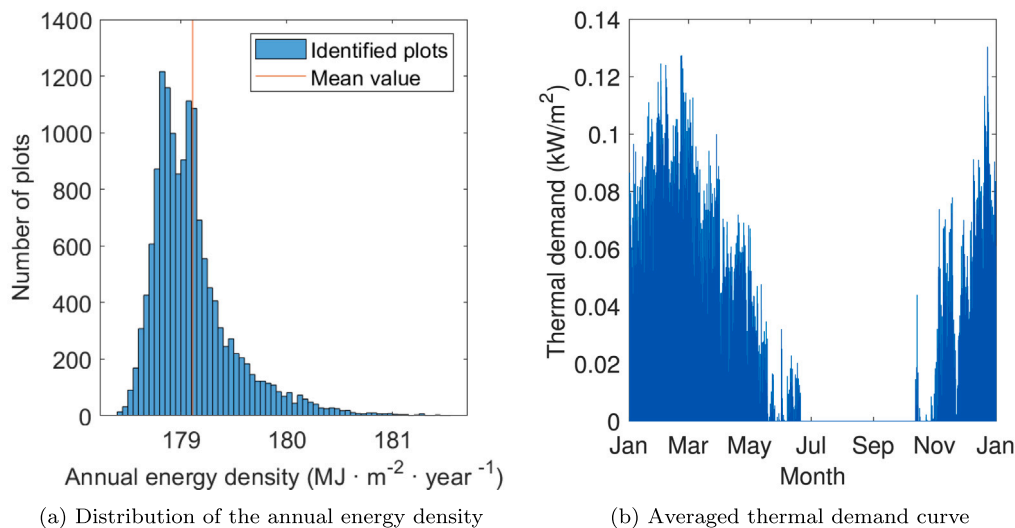


Fig. 6. Analysis of the thermal needs for all the plots corresponding to greenhouses in El Ejido.

2.3. Optimal routing

As mentioned above, the network layout is determined by selecting points of consumption (plots of land) that are more favorable from the economic point of view. Except for the node corresponding to Ence's plant, the graph defined in Section 2.2.1 contains nodes that are part of the road network, some of which are points of supply connected to the said points of consumption. The rest of the nodes just encode the possible routes between the points of supply and the plant (single point of production) in the graph. Fig. 7, on which further detail is provided throughout this section, illustrates the three-stage approach used to get the network layout, where the first stage includes the use of a genetic algorithm to both initialize the population and obtain the optimized population, the second corresponds to the calculation of the cost function employed by the said algorithm, and the third is devoted to solving the minimum Steiner tree required to calculate the cost of the network.

Considering that the selection of a certain point of supply implies the selection of the points of consumption connected to it, the problem addressed in this section consists in determining a subset of nodes, corresponding to points of supply, that maximizes a certain economic indicator of the profitability of the thermal network: the Net Present Value (NPV) of the possible solutions (see Section 2.4). In other words, it is about solving an optimization problem in which the cost function is given by the NPV and for which a genetic algorithm is used, as illustrated in Fig. 6(a). At this point, it is essential to acknowledge that genetic algorithms have proven successful in studies involving other design features related to heating networks' layout [39,40]. In this case, the decision variables of the problem are binary and represent whether or not a certain point of supply is selected to be part of the network, hence each individual in the population represents a subset of connected points of supply (a subgraph of the original graph).

As the most influential factor, when it comes to the investment and operational costs, is the total length of the network (see Section 2.4), the resulting subgraph needs to have the minimum essential length to connect the points of supply/production. In terms of graph theory, if the weight of the edges of the graph is defined as the geographical distance between two points of the road network (see 2.2.1), then one condition that such subgraph needs to meet is that, regardless of the nodes corresponding to points of production or supply, all its nodes must be connected without loops and in such a way that the total sum of weights is the minimum possible (thus minimizing the total length of the network). Determining a subgraph that meets the above condition is known as the Steiner tree problem and this subgraph is called the

minimum Steiner tree or MST, an acronym also used in the literature for the minimum spanning tree (not in this article).

Since reaching the optimal solution to the MST problem is not computationally possible in polynomial time, this problem is usually simplified based on the minimum spanning tree [41]. Similarly to other previously published papers on district heating networks [5,7], a simplified algorithm is implemented in the MATLAB programming environment, as explained in Appendix B. This approach consists of the following steps: (i) the application of a Delaunay triangulation, to determine between which points of supply or production the edges of a new graph are generated; (ii) the use of Dijkstra's algorithm, to calculate the weight of the edges; (iii) the execution of Kuskal's algorithm, to obtain the minimum spanning tree. Despite the possible convergence to suboptimal solutions, there is a fundamental reason to use this method instead of others that try to obtain the actual MST: the problem can be solved in polynomial time. However, unlike the cited papers, in which the points of supply/consumption are predetermined [5,7], in this work a genetic algorithm (see Section 2.4) is used to generate populations of candidate solutions on which the simplified Steiner tree problem is solved (see Appendix B).

Genetic algorithms are a set of metaheuristic optimization techniques based on an iterative improvement process, through recombination and mutation of existing solutions, by selecting individuals that minimize a particular cost function. They try to imitate natural selection, where the best-adapted individuals survive whereas the rest do not. The MATLAB programming environment provides the *ga* function [34], expressly designed to apply this optimization algorithm, which is used in this work. It is worth mentioning that, in Fig. 7, two sections corresponding to the same genetic algorithm are shown. This is because the genetic algorithm is executed twice with different configurations to reduce the computational effort in finding solutions. As the results of this technique are highly dependent on the initialization values of the population, the following process described below is carried out.

First, a new "nodes" file is generated in QGIS, in which all the points of supply at a distance greater than 2 km from Ence's plant are redefined as simple points of the road network. This reduces the optimization problem by having only 733 points of supply (decision variables) instead of 14 085. Subsequently, the genetic algorithm described in Section 2.4 is executed on this layer of nodes with the default configuration for *ga* [34], except for the following parameters: (i) parallelized computing (*UseParallel* parameter), which is activated to reduce the computation time of the algorithm; (ii) the size of the population (*PopulationSize* parameter), which is set to 1000 individuals; (iii)

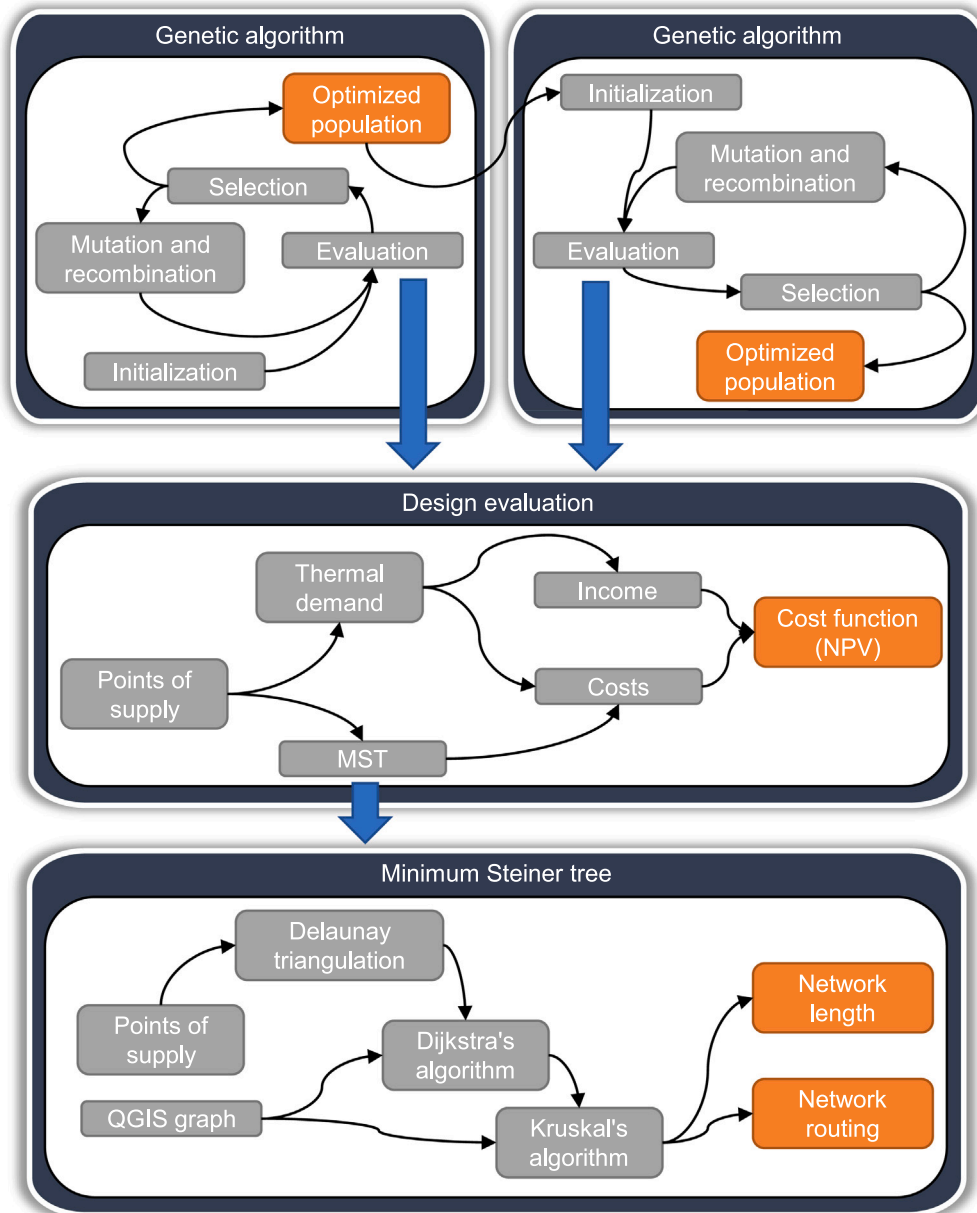


Fig. 7. Descriptive diagram of the strategy for obtaining the optimal network layout consisting of three stages.

the maximum number of recessive generations (*MaxStallGenerations* parameter), which is set to 1000 and; (iv) the matrix that defines the initial population (*InitialPopulationMatrix* parameter), in which the individual corresponding to “not building the network” is defined, with NPV equal to 0 €. Until completing the population size, the rest of the individuals are defined randomly according to the default configuration for ga function [34].

Second, and from the previous point, the optimized individuals with NPV greater than 0 € (profitable projects with points of supply within a radius of 2 km from Ence’s plant) are kept and used to initialize a new matrix that defines the initial population. The genetic algorithm is executed again (with identical configuration except for the said matrix) considering the 14 085 points of supply of the municipality (with the file described initially in 2.2.1). This generates a new optimized population in which the best individual (the one with the highest NPV) is chosen to design the thermal supply network.

In this way, the computation time and the number of explored candidate solutions are considerably reduced since the random generation of individuals results, in general, in highly unprofitable projects. For the first search, the individual defined in the initial population as a borderline project (NPV equal to 0), is likely to be recombined with others when the population is made up of many unprofitable projects. For the second execution, with an increased computational burden as the number of decision variables is multiplied by twenty, the algorithm hopefully counts at the start with a set of profitable projects concentrated around Ence’s plant, on which to explore whether it is more or less profitable the expansion into new points of supply.

2.4. Cost function

As introduced in the previous paragraphs, obtaining points of supply (and indirectly points of consumption) to determine the layout of the network is based on solving the optimization problem presented

in Eq. (10):

$$\begin{aligned} \min \quad & -NPV(\mathbf{x}) \\ \text{s.t.} \quad & \mathbf{Q}_{dem} \cdot \mathbf{A}' \cdot \mathbf{x} \leq \mathbf{Q}_{net} \cdot \eta_{net} \end{aligned} \quad (10)$$

where \mathbf{x} is a vector of $N \times 1$ binary elements (value 0 or 1) that represents, from the set of points of supply of the graph described in 2.2.1, which are part of the supply network (value 1); N is the total number of points of supply (14 085); NPV is a function that returns the net present value of the thermal network as a function of \mathbf{x} , that is, the points of supply selected to be part of it; \mathbf{A} is a vector of size $N \times 1$ whose elements are the area corresponding to each point of supply (the sum of the areas of the points of consumption that are grouped in that point of supply); \mathbf{A}' denotes the transpose of vector \mathbf{A} ; \mathbf{Q}_{dem} is a vector of size 8760×1 whose elements are the thermal power demanded per surface unit for each hour of the year (defined from the curve in Fig. 6(b)); \mathbf{Q}_{net} is a vector of size 8760×1 whose elements are the thermal power available to the network at each hour of the year (defined from Eq. (2)); η_{net} is the thermal efficiency that considers the heat losses by distribution, taking a value of 0.7596 as justified below (see Eq. (19)).

The NPV is an indicator used in investment decisions, which contemplates the future cash flows of a project over time, to determine “the profitability of a projected investment or project” [42]. To estimate the current value of all cash flows, a discount rate is used, whose value is usually equated to the cost of capital or the minimum gross return required for the project [43]. Calculating NPV via Eq. (11) is possible thanks to the availability of methodologies to estimate the investment and operational costs and the income obtained from the sale of energy to consumers, as explained below.

$$NPV(\mathbf{x}) = -C_{inv}(\mathbf{x}) + \sum_{t=1}^n \frac{p \cdot E(\mathbf{x}) - C_{op}(\mathbf{x})}{(1+i)^t} \quad (11)$$

In Eq. (11), C_{inv} are the initial investment costs of the network, which are a function of the layout, and therefore of the points of supply selected according to \mathbf{x} ; E is the energy that would be consumed annually at the selected points of supply, and therefore a function of \mathbf{x} ; p is the sale price of the energy consumed, for which, in the design of the network, a constant conservative value is considered, as explained below; C_{op} are the annual operational costs of the network, which are a function of the layout, and therefore of the points of supply selected according to \mathbf{x} ; i is the discount rate used to estimate the present value of all cash flows; n the number of years corresponding to the useful life of the project.

Some considerations should be made for the above expression: (i) the thermal network is considered not to have any residual value at the end of its useful life, as it is a specific infrastructure and hard to dismantle; (ii) since the expression provides a positive value when the project is economically viable, Eq. (10) requires to include the NPV with a negative sign to set the minimization objective correctly; (iii) a useful life of 30 years is considered, as it is the minimum required for pipes according to the EN 253 standard [44], although up to 50 years could be considered according to Cofely’s guide [19]; (iv) initially, a discount rate of 3% is considered, although, for more rigorous analyses, the financial situation of potential developer would have to be considered.

Firstly, the annual energy consumption (for an 8760-hours period) of the selected points of supply can be calculated according to Eq. (12):

$$E(\mathbf{x}) = \mathbf{Q}'_{dem} \cdot \mathbf{1} \cdot \mathbf{A}' \cdot \mathbf{x} \quad (12)$$

where $\mathbf{1}$ is a vector of 8760×1 elements with value 1, used to aggregate the power demanded throughout the year; \mathbf{Q}'_{dem} denotes the transpose of vector \mathbf{Q}_{dem} . Because \mathbf{Q}_{dem} is expressed in kW/m^2 for hourly intervals, the units of $E(\mathbf{x})$ are kWh year^{-1} .

On the other hand, the sale price of energy consumed is initially set at 0.05 €/kWh, which is considered an attractive value for potential interested parties, as justified below.

- Although, as Cofely’s guide clarifies, a project can be executed by public administrations, a cooperative of consumers (i.e. farmers), or private entities (Ence or any other company that acts as an intermediary), it makes more sense for the approach of this work to consider the latter case, since the design is based on the selection of the most favorable points of supply. For a cooperative or public administration, it is more likely that the points of supply will be predetermined.
- Assuming that the projected activity for Ence’s plant would be profitable solely thanks to the sale of electricity, the costs of generating the heat that would be injected into the network would be covered (fuel at zero cost). For this reason, the objective of the energy price should only contemplate, in addition to the business benefit, the operation and amortization of the network, hence the price may be reduced in comparison with other sources of energy.
- In the studies analyzed, a price of 0.05 €/kWh is considered for gas in the design of a district heating network [5] and 2.41 €/m² for a diesel-heated greenhouse [14]. For the second case, if the energy cost is calculated considering the average annual energy density obtained in Section 2.2.2 (179.11 MJ m⁻² year⁻¹), a similar price would be obtained (0.0484 €/kWh).

Regarding the cost analysis, although some authors also consider the cost of fuel [45], since this is considered to be nil, as previously justified, the following categories can be established: (i) investment costs; (ii) distribution costs, usually distinguishing between heat and load losses and; (iii) maintenance costs, which are neglected as in other works because they are practically irrelevant compared to the rest of the costs [45,46].

The calculation of investment costs based on the so-called “linear heat density” of the network, which depends on the energy sold annually and the length of the network, is recurrent in the literature [46]. Therefore, a detailed design is not required to assess the costs, only the network extension and the points of supply. Formulas in [46] have been recently updated for several countries of the European Union [47] and used in studies of a similar nature to this work [5,48], remaining according to Eqs. (13) and (14):

$$C_{inv}(\mathbf{x}) = L(\mathbf{x}) \cdot (C_1 + C_2 \cdot d_a(\mathbf{x})) \quad (13)$$

$$d_a(\mathbf{x}) = 0.0486 \cdot \ln \left(\frac{E(\mathbf{x}) \cdot 3.6 \cdot 10^{-3}}{L(\mathbf{x})} \right) + 0.0007 \quad (14)$$

where C_1 and C_2 are two experimental coefficients based on the country, with their values being 354 €/m and 4314 €/m² respectively for the case of Spain [47]; L is the total length of the network (expressed in meters), calculated from the selected points of supply (according to \mathbf{x}), as explained in Appendix B; d_a is the average pipe diameter (expressed in meters), obtained from the equation by Persson and Werner [46], including the conversion factor from kWh to GJ.

As for heat exchange, in the study by Lumbreras et al. [5], a fixed cost of 2500 € is assigned to each point of supply or substation [49], a value quite different from the minimum proposed in Cofely’s guide [19], which is around 22 000 €. The reason for this difference may lie in the power considered for each substation, which, according to the Danish Energy Agency, is affected by economies of scale: greater power results in a lower price per kilowatt [50]. Thus, in this work, Eq. (13) is redefined to consider the existence of substations at points of supply, as expressed in Eq. (15), and Eqs. (16) and (17) are added, in order to calculate their cost is based on an experimental fitting with the previous data (see Fig. 8):

$$C_{inv}(\mathbf{x}) = L(\mathbf{x}) \cdot (C_1 + C_2 \cdot d_a(\mathbf{x})) + C_{sub}(\mathbf{x}) \quad (15)$$

$$\mathbf{Q}_{sub}(\mathbf{x}) = \max(\mathbf{Q}_{dem}) \cdot \mathbf{A} \cdot \mathbf{diag}(\mathbf{x}) \quad (16)$$

$$C_{sub}(\mathbf{x}) = \sum_{j=1}^N C_{sub}^j = \sum_{j=1}^N b \frac{Q_{sub}^j}{Q_{sub}^j + a} \quad (17)$$

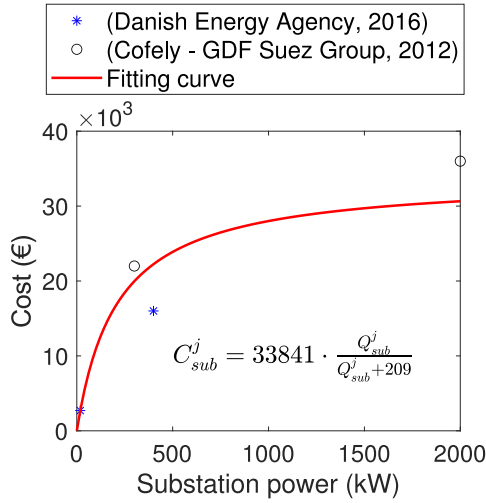


Fig. 8. Fitting curve obtained to calculate the cost of a substation based on its power.

where C_{sub} represents the total cost of the substations required for the selected points of supply according to \mathbf{x} ; \mathbf{Q}_{sub} is a vector of size $N \times 1$ whose elements are the maximum demanded power by each point of supply; max is a function that returns the maximum value among the elements in \mathbf{Q}_{dem} ; $diag$ is a function that returns \mathbf{x} in form of a diagonal (in other words, creates an $N \times N$ diagonal matrix with binary elements that represent, from the set of points of supply in the graph described in 2.2.1, which ones are part of the supply network); C_{sub}^j is the cost of the substation at the point of supply j ; Q_{sub}^j is the j th element of \mathbf{Q}_{sub} (the maximum demanded power by the point of supply j); a and b are two coefficients adjusted experimentally, as shown in Fig. 8 (with values of 209 kW and 33 841 €, respectively).

For the curve in Fig. 8, some fitting indicators have been calculated: the mean error is 289 €, the root mean square error is 4237 €, and the coefficient of determination R^2 is 0.8834. Note that the samples correspond to data from the previously mentioned sources, which present different price scales. In the case of the Cofely guide, only the minimum (300 kW, 22 000 €) and maximum (2000 kW, 36 000 €) values have been considered.

To consider distribution costs (heat and load losses), a report for Northern European countries performed by the IEA has been considered [51], which constitutes a conservative approach regarding the geographical area of this work (assuming the same construction materials, there would be lower losses/costs due to the warmer Almerian climate). According to the said report, heat losses (Q_{loss}) can be calculated by using Eq. (18):

$$\frac{Q_{loss}(\mathbf{x})}{E(\mathbf{x}) + Q_{loss}(\mathbf{x})} \cdot 100 = 17 \cdot \left(\frac{E(\mathbf{x}) \cdot 10^{-3}}{L(\mathbf{x})} \right)^{-0.5} \quad (18)$$

where the left-hand term expresses the heat losses as a percentage of the total produced heat, and the fraction on the right-hand side represents the previously mentioned linear heat density (including a conversion factor from kWh to MWh). Since the generation costs of the injected heat into the network are assumed to be covered (fuel at zero cost), heat losses (Q_{loss}) do not directly affect operational costs (C_{op}), but they do indirectly impact the plant design, as reflected in the thermal efficiency of the network (η_{net}) in Eq. (10). This efficiency can be calculated by means of Eq. (19),

$$\eta_{net}(\mathbf{x}) = 1 - \frac{Q_{loss}(\mathbf{x})}{E(\mathbf{x}) + Q_{loss}(\mathbf{x})} = 1 - 0.17 \cdot \left(\frac{E(\mathbf{x}) \cdot 10^{-3}}{L(\mathbf{x})} \right)^{-0.5} \quad (19)$$

hence it is a function of the selected points of supply according to \mathbf{x} . However, to avoid introducing a relationship in Eq. (10) that would significantly increase the genetic algorithm's computation time (as this

constraint would require solving the MST problem in order to calculate L , as explained in B), the following arrangements are made: (i) a minimum linear heat density value of 0.5 MWh/m is set—which is consistent with Eq. (14) and the observations used for Persson and Werner's fitting [46]—and the corresponding efficiency ($\eta_{net} = 0.7596$) is calculated using Eq. (19); (ii) the said efficiency value is considered in Eq. (10) to obtain the available power for consumers; (iii) a condition is introduced into the cost function to associate any network design with a linear heat density below 0.5 MWh/m with a Net Present Value (NPV) of $-1\,000\,000$ €.

The above procedure addresses the elimination of designs with low linear heat densities and efficiencies worse than 0.7596, since a project with a negative NPV is not viable compared to a situation with “zero cost”, where the project would not be carried out. Whilst this simplification might lead to slightly less optimal results, the computation time until convergence is exponentially reduced by removing the dependency on L in the constraint. Furthermore, this approach deals with another issue arising from Eqs. (13) and (14): as the linear heat density decreases, so does the value of d_a and the total project cost. Therefore, without bounding the value of linear heat density as has been done (or introducing additional constraints), solutions with absurdly long networks could be reached, where the pipe diameter becomes negative (with densities on the order of 0.01 MWh/m). The choice of 0.5 MWh/m as the minimum value for linear heat density is based on the minimum pipe diameter value (0.0293 m) for the observations in Persson and Werner's study [46].

Regarding costs due to load losses (or costs of electricity consumed by pumping the heat transfer fluid), the IEA report suggests that the electrical energy consumed is around 1% of the thermal energy supplied to the network [51], as expressed in Eq. (20):

$$C_{op}(\mathbf{x}) = \frac{0.01}{\eta_{net}(\mathbf{x})} \cdot E(\mathbf{x}) \cdot c \quad (20)$$

where c is the cost of the electricity that Ence would not sell in order to operate the thermal supply network, and η_{net} is calculated for each candidate solution by means of Eq. (19). A constant value of 0.17 €/kWh is considered for c , which is the average price in the day-ahead market for the year 2022, according to data from the Spanish market operator [52].

2.5. Economic sensitivity analysis

Given that many of the assumptions made in this work are not free from uncertainty, it is interesting to analyze how the project's profitability can vary when some of the main variables involved in the calculation of NPV are modified (see Section 2.4), and a sensitivity analysis is conducted on the proposed final layout for the district heating network, considering the following variables.

Regarding \mathbf{Q}_{dem} , the energy density estimated from the model in Section 2.2.2 is based on a number of assumptions. Whether an increase in the thermal demand due to using higher temperature setpoints or a decrease because the model might be overly optimistic in selecting certain parameters, they would affect the NPV and hence further analysis on its impact is required.

In practice, the price p set in Section 2.4 would be better determined by analyzing the horticultural and energy markets. For instance, according to data from 2013 in the study by Valera et al. at that time, the price of tomatoes was high compared to the price of fuels. The authors explain that with an “average tomato price of 0.61 €/kg” and an “average diesel price of 1.03 €/L”, the “fruit production increase of 0.86 €/m²” was much lower than the cost of consumed fuel for heating (2.41 €/m²) [14]. From that data, the authors of this work consider that reducing the energy price by at least 65% (0.017 €/kWh instead of 0.0484 €/kWh) could make heating systems attractive for farmers. The opposite case is also of interest: how profitability would increase if energy can be sold at a higher price (e.g. due to a booming horticultural market), as is analyzed for other networks [5].

Finally, the discount rate set in Section 2.4 (i) is intended for minimal profit in an ideal case of unencumbered capital and a moderately inflationary environment of 2%, believed to be beneficial for the economy and the objective of central banks like the European and American ones [53]. However, numerous scenarios (financial strategy, alternative investments, deflationary economic environment, etc.) can influence the appropriate value for this variable, hence its effect is analyzed across a wide range of values.

The rest of the variables are not considered in the sensitivity analysis either because of their minimal impact on the NPV or because the uncertainty associated with them is relatively low. For example, the price of electricity c , subject to variations throughout the year, affects operational costs, but these costs are nearly an order of magnitude lower than the annual revenues. The areas of the plots in A may not exactly correspond to the actual heated surface, but it is trusted that SIGPAC has delimited each greenhouse with sufficient precision.

3. Results

All calculations have been carried out on a desktop computer equipped with an Intel® Core™ i7-6700K 4 GHz microprocessor, NVIDIA GeForce GTX 1070 graphics card, 16 GB of RAM, Samsung SSD 970 EVO 1 TB hard drive, and Windows 10. Some of the most demanding operations in QGIS took several hours, whereas the computation time of the genetic algorithm was 4.1045 h for the reduced problem (using only the points of supply within a radius of 2 km from Ence's plant) and 2.9608 h for the entire municipality. The fact that the computation time is lower in the second case, when it would be expected to be much higher due to the larger search space, is justified by the termination criteria of the algorithm and by the absence of individuals with better performance (higher NPV). In both cases, the algorithm terminated with $exitflag = 1$, which according to the documentation of the ga function [34] means that the average variation in the cost function is less than the defined tolerance, without violating the constraints.

3.1. Analysis of optimized populations

In Fig. 9, heat maps are presented for the two optimized populations, indicating how many times a particular plot is part of any of the individuals. Note that, as this is an optimization problem involving integer variables, the populations may contain individuals that violate the constraint imposed in Eq. (10), according to the documentation of the ga function [34]. For this reason, to analyze the results obtained, it is necessary to filter only those feasible individuals (those that meet the demand–availability constraint in Eq. (10)) and with a positive NPV (profitable projects). In the case of the algorithm that runs on the points placed within a radius of 2 km from the centroid of the plant (Fig. 9(a)), a series of selected plots can be observed around it. Oppositely, light blue indicates plots that have not been selected for any individual. The population contains 341 individuals, hence there are many alternative projects in which a different plot is selected. The interpretation for the entire municipality (Fig. 9(b)) is similar, except for a fundamental difference: the number of feasible individuals (with a positive NPV) is only 5, due to the much larger search space, and, since no individuals with better performance have been found, the plots are restricted to cases practically identical to the final design (see Fig. 12).

Fig. 10 shows the relationship between the total length of the network, the main design variable, and the net present value (NPV) of each individual (project) for the two optimized populations. As shown in Fig. 10(a), there seems to be a threshold around 1.3–1.5 km for which a project is more profitable. This is because, with shorter lengths, the network would not supply a sufficient number of plots due to the geographic distances between them, and, with longer lengths, the network cannot supply more plots due to the limited available power

Table 3

Characteristics of the proposed thermal network.

Description	Variable	Value
Net present value of the project	NPV	6.4179 M€
Total initial investment costs	C_{inv}	1.7233 M€
Cost of substations	C_{sub}	0.3569 M€
Annual operational costs	C_{op}	0.0158 M€ year ⁻¹
Annual supplied energy	E	8621.4 MWh year ⁻¹
Income from annual energy sales	$p \cdot E$	0.4311 M€ year ⁻¹
Total length of the network	L	1.3464 km
Average pipe diameter	d_a	0.1532 m

(Eq. (10)). Therefore, the NPV tends to decrease below and above that threshold, as also reflected in Fig. 10(b).

In addition, the existence of this threshold justifies the scarcity of profitable projects when considering all the points of supply in the municipality: since the geographic extension and the number of combinations are much larger, it is very likely that the population will evolve by incorporating individuals that are less well adapted (with lower NPV). Although, in light of these results, it would be possible to execute the genetic algorithm again with parameters that favor a greater number of recombinations (such as larger population size), the fact that the threshold for optimal projects is far below the 2 km radius is reason enough to dismiss investing more resources in a new calculation, which would also be even more computationally expensive.

Finally, with regard to the general characteristics of the optimized population for the reduced problem, it should be noted that there is a significant number of projects that could be profitable. Most of them represent networks of length between 2 and 6 km and an NPV of 2 to 4.5 million euros, as shown respectively in Figs. 11(a) and 11(b). In the following sections, only the results for the best-performing individual of both populations (the one with the highest NPV) are presented and analyzed in detail.

3.2. Design proposal and sensitivity analysis

According to the results obtained after the double execution of the genetic algorithm, a network of 1.3464 km would be responsible for supplying 8621.4 MWh of heat annually to 12 points of supply, each corresponding to a plot located to the northwest of the plant (see Fig. 12). Its characteristics are summarized in Table 3, which also breaks down the different cash flows through which an NPV of 6 417 900 € is obtained. Table 3 shows that operational costs are significantly lower than annual income, which is why many authors do not take them into account. The costs related to the substations are an important part (20.71%) of the total investment costs and are considered in the subsequent sensitivity analysis, as explained below.

In regard to operational constraints, Fig. 13(a) shows the thermal availability at the points of consumption, that is, the result of Eq. (2) weighted by the network efficiency, versus the total consumption of the 12 selected plots. From March to June and from October to December, the availability of heat is much higher than the demand, which means that there would be room for improvement, by setting an availability curve that better fits the demand and allows the network to supply heat to more plots. However, determining that curve would require much greater knowledge about the operation of Ence's plant and even imposing planning conditions on it.

Regarding the substations needed for the network, Fig. 13(b) illustrates the nominal power values and cost of each substation according to the curve shown in Fig. 8. Except for two of the substations (with powers of 2999.5 kW and 6124.5 kW) that involve extrapolation from available data, the rest of them would better fit within the price range exposed in Cofely's guide (as opposed to the Danish Energy Agency's guide). Since the fitting curve underestimates the prices of the former and overestimates those of the latter, readers might wonder what would happen if the substations' actual prices differ from those in the final

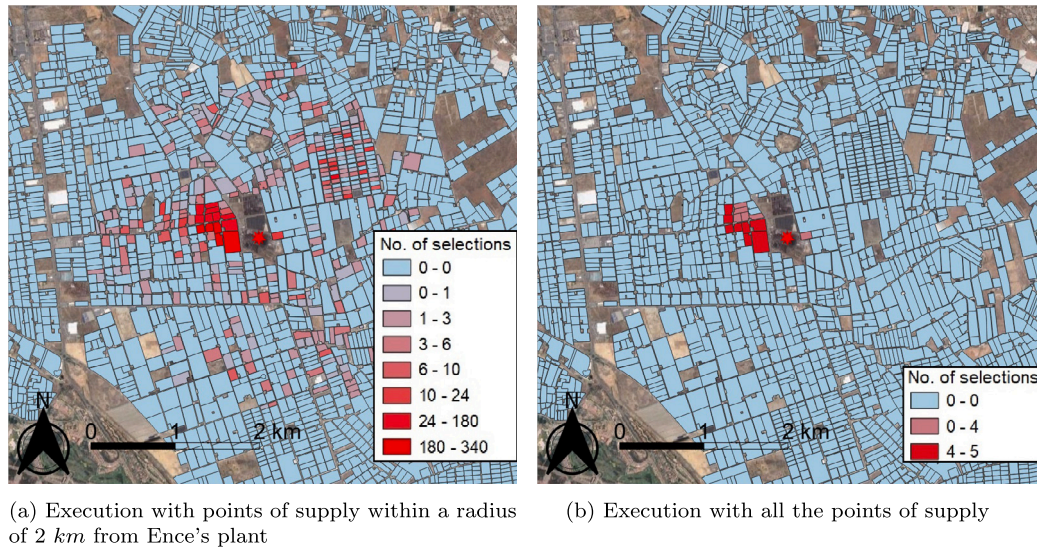


Fig. 9. Heat map showing the plots selected by the genetic algorithm a higher number of times in the different optimized populations.

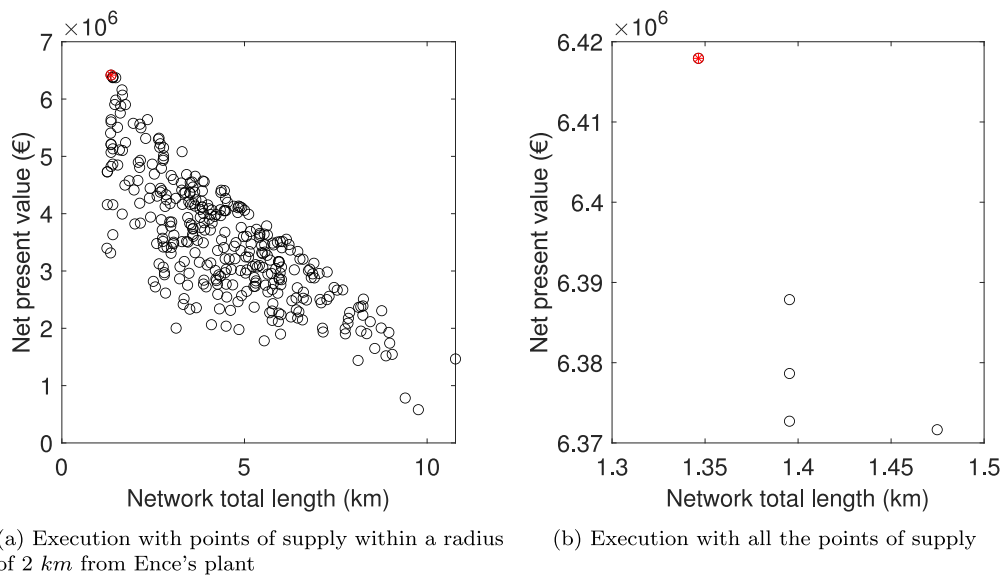


Fig. 10. Net present value as a function of the total length of the network for individuals in the optimized populations (in black) and for the final design (in red). (For interpretation of the references to color in this figure legend, the reader is referred to the web version of this article.)

design. To throw light on this issue, the cost of the substations in Table 3, 356 900 €, can be compared with a somewhat extreme case: considering that 14.5 substations of 2000 kW (ten within the range of Cofely's guide and an equivalent number of 4.5 stations for the two extrapolated ones) are built at a cost of 36 000 € each (the maximum price and power according to the guide's data). In that case, the total cost of the substations would be 522 000 €, an increase of just 165 100 € over the total investment costs in Table 3, which would have a negative (but practically insignificant) impact on the NPV.

Finally, Figs. 14(a), 14(b), and 14(c) show how the NPV of the final design would evolve when some of the variables that have the greatest impact on the economic model are modified, as discussed in Section 2.5. In Fig. 14(a), the curve asymptotically decreases to a negative NPV equal to the total initial investment costs when the discount rate tends to infinity. Values are only presented in a reasonable range for the discount rate, between 0 and 0.15, for which the NPV remains positive, and hence the project would be profitable, assuming no changes occur in the other two variables analyzed. In Fig. 14(b), the variable with the highest degree of sensitivity in the model is

observed, that is, the price at which thermal energy is sold from the network to consumers. This variable has a strictly linear relationship with the NPV, which only falls below zero when the price is below 0.0121 €/kWh. This implies that in an unfavorable situation, such as the one presented in Section 2.5, where the price might need to be reduced to 0.017 €/kWh to maintain demand levels, the project would still be profitable, assuming no changes occur in the other two variables analyzed. In Fig. 14(c), the relationship between thermal energy demand and NPV is shown. Energy demand is expressed in percentages, considering that 100% is equivalent to the demand curve used for the 12 plots (Fig. 13(a)), and the restriction imposed on the power curve is neglected for this analysis. An approximately linear relationship is shown, with a clear discontinuity for values below 8%, for which the linear heat density is less than 0.5 MWh/m and therefore the NPV takes values of -1 000 000 €, as explained in Section 2.4. For demands below 12% of the original demand, NPV also takes negative values.

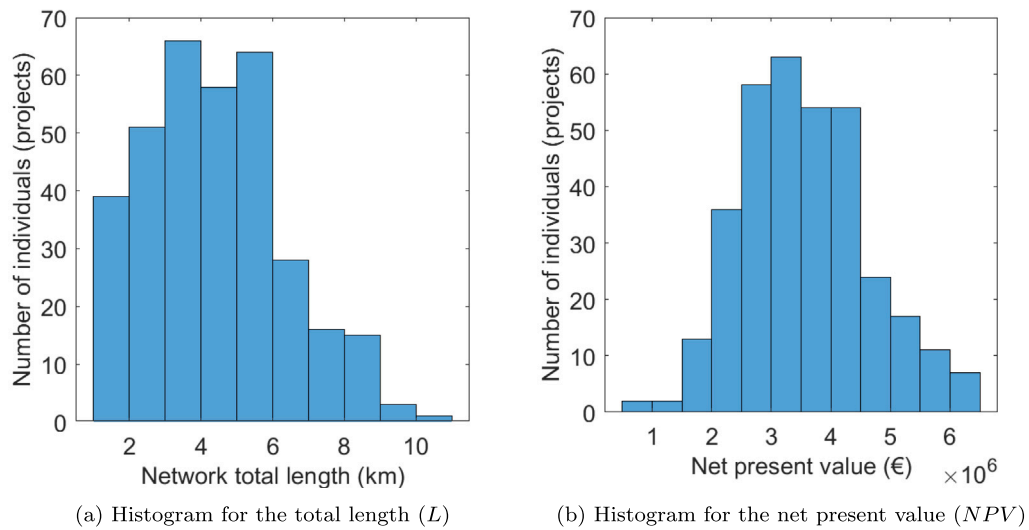


Fig. 11. Distributions for the optimized population corresponding to the execution with points of supply within a radius of 2 km from Ence's plant.

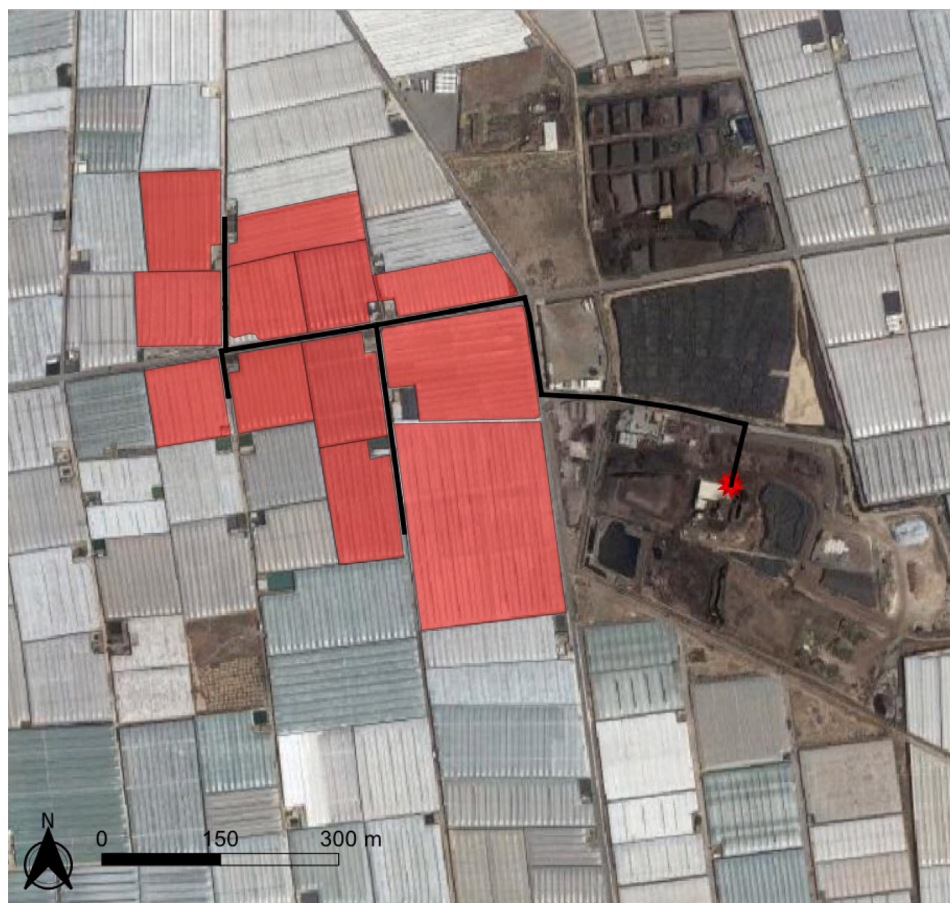
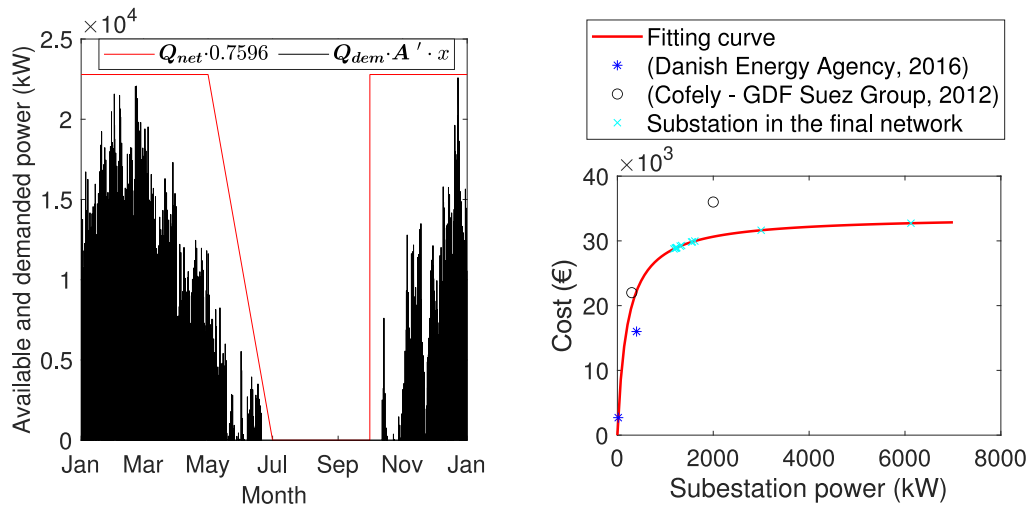


Fig. 12. Final layout of the district heating network and selected plots (in red). (For interpretation of the references to color in this figure legend, the reader is referred to the web version of this article.)

4. Conclusions

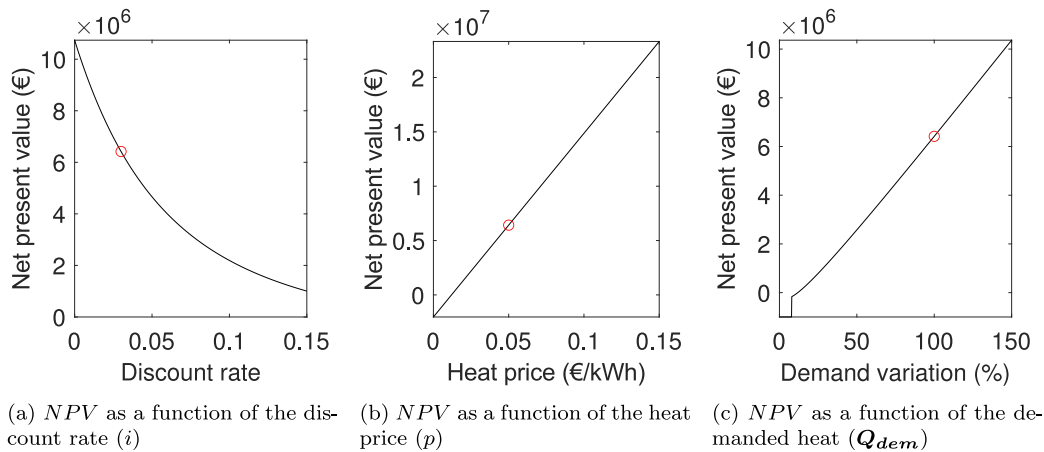
As stated in Section 1, this paper presents the layout, sizing, and preliminary cost structure of a thermal supply network that provides energy to 12 plots located at the northwest corner of the plant that the company Ence Energía y Celulosa, S.A. plans to build in El Ejido [15].

Although the results obtained from the economic analysis are encouraging, implementing a thermal network like the one proposed in this article is not exempt from complications for the plant's operation. To produce heat and power, Ence would have to consider not only the needs of the drying process but also the thermal demand of the network's users. This might reduce the flexibility of the operation but, on the other hand, offers an alternative for useful heat that either would



(a) Thermal demand curve of the selected plots (in black) and available power for the network (in red) (b) Cost and power of the twelve substations

Fig. 13. Annual energy planning and substations corresponding to the final design.



(a) NPV as a function of the discount rate (i) (b) NPV as a function of the heat price (p) (c) NPV as a function of the demanded heat (Q_{dem})

Fig. 14. Evolution of the net present value of the project corresponding to the final design (red circle) against changes in the main variables. (For interpretation of the references to color in this figure legend, the reader is referred to the web version of this article.)

reduce the cogeneration plant's efficiency (with a negative impact on the legal bonuses for efficiency reasons) or would result in the accumulation of dried biomass. An interesting study for the company might also delve into the relationship between the price set for energy sales and the increase or decrease in demand. This would serve both to determine new operation strategies and to reduce the uncertainty of the economic model used in this work.

Since this work offers a preliminary analysis, some simplifications have been made when estimating the potential thermal demand of the greenhouses. In order to determine a more realistic demand curve, the following improvements deserve to be mentioned.

- By analyzing both the digital terrain model and the digital elevation model of El Ejido, the height of each greenhouse could be estimated more accurately. This was not deemed relevant for this paper, given the homogeneity of heights, but it is not negligible when it comes to urban environments with all kinds of buildings [5].
- Image analysis could be used to determine the geometry of each greenhouse (e.g. Almería-type, tunnel-type...), which would help to better determine the thermal needs.
- PVGIS provides the typical meteorological year (TMY) with a limited geographical resolution. It could be interesting to incorporate

data from local weather stations throughout the municipality to adjust the TMY based on individual plots or groups of plots.

- SIGPAC's data does not contain information on the owner of each plot, so incorporating data from the land registry might be fruitful, as that would allow the identification of owners of adjacent plots that may require a single point of supply for all of them (rather than a different point of supply per greenhouse centroid).
- The temperature setpoints used in this work are applicable to a wide variety of crops commonly grown in the region, but a more accurate analysis could consider the area dedicated to each type of crop throughout the year/season to integrate all their thermal needs into a crop-weighted demand curve.

Furthermore, it is crucial to acknowledge the limitations associated with costs, since this study remains agnostic about soil conditions: the calculation of investment costs is derived from Persson's study [46], and their approach involves a regression analysis based on some network characteristics, without considering other geographical conditions that affect trenching costs. In this regard, the soil type, water content, depth of cut, or surcharge loads, among others, can have a significant impact on the expenses. For instance, a rocky terrain may require specialized digging equipment, or high water content in clay soils could

imply additional dewatering measures, which introduces variability in Persson's equations. Addressing these practical considerations comprehensively, as a part of a posterior detailed design, is essential for accurately assessing the feasibility and cost-effectiveness of the project.

Finally, regarding the application of the methodology developed to other similar contexts, the same analysis could be carried out from the perspective of a cooperative of farmers and/or public administrations as the developer of the project, in which case: (i) it would probably be necessary to include in the economic model situations in which the owners already have or are considering installing an individual heating system and its impact in terms of possible savings; (ii) the design could encompass the so-called "secondary network", i.e., considering in the routing the length from each point of supply to the plot centroid or point of interest for each owner. Also, owing to the limitations of heat production from Ence's plant, other situations have not been explored in depth, but future work could consider the following cases: (i) the implementation of a heating and cooling network, also considering the thermal needs of the greenhouses during the summer period; (ii) the inclusion of urban and/or industrial areas to determine new potential points of supply and their respective demand curve; (iii) the consideration of more than one source of thermal energy.

CRedit authorship contribution statement

Jerónimo Ramos-Teodoro: Writing – original draft, Software, Methodology, Investigation, Data curation, Conceptualization. **José Domingo Álvarez:** Writing – review & editing, Writing – original draft, Validation, Supervision, Funding acquisition, Formal analysis. **José Luis Torres:** Writing – review & editing, Writing – original draft, Validation, Supervision, Funding acquisition, Formal analysis.

Declaration of competing interest

The authors declare that they have no known competing financial interests or personal relationships that could have appeared to influence the work reported in this paper.

Data availability

All the data used in this article is available from the third-party providers cited along the text. MATLAB data and code is available "as is" through the GitHub repository linked in the article.

Acknowledgments

This work was carried out as part of the Project MICROPROD-SOLAR (acronym for "Microrredes para el autoabastecimiento solar de entornos productivos aislado") funded by the International Joint Programming initiative of the State Research Agency of the Spanish Government, grant PCI2019-103378, and by the Iberoamerican Program for Science and Technology for the Development (CYTED).

Appendix A. Estimation of the thermal needs for drying

To determine Q_{dry} in Eq. (1), the most unfavorable case is first considered, that is, when the plant dryer is operating at its maximum capacity, with the input of wet biomass being 150 000 kg/h or the output of dry biomass being 120 000 kg/h [23]. Since the dryer is made of a belt system that uses air as a drying medium, Table A.4 compiles the parameters of Ence's plant together with those provided by other authors for this type of systems [54].

Because the input and output capacities of the dryer previously exposed are not consistent with the humidity percentages provided by Ence (from an input humidity of 52%, an output humidity of 40% would be obtained) and in the AAI/AL/142/22 the evaporation capacity is not specified, this is estimated as follows: from the wet

biomass input flow of 150 000 kg/h (with 52% humidity) the output flow is calculated so that the dry biomass has a 25% humidity. Thus, the dryer would yield an output flow of 96 000 kg/h and a water evaporation rate of 54 000 kg/h.

With the above data, and assuming an energy demand of 5 MJ per kg of evaporated water, the thermal power required for the dryer in the worst case scenario would be 75 MW, so by substituting in Eq. (1), the availability of thermal power for the distribution network would be 0.36 MW. Although this value seems insufficient for a thermal network of some entity, it happens that the arrival of fresh biomass is concentrated in a few months of the year (May, June, and July), as recognized by Ence itself, which over-dimensions its biomass processing facilities with respect to those for energy generation [23]. Therefore, the demand for thermal power for the dryer (higher in spring–summer months) and for the thermal network (higher in autumn–winter months) are decoupled in time and it can be considered that the dryer does not operate all year at its maximum capacity.

In particular, the largest volume of biomass, 75% of the total, corresponds to spring and long-cycle crops, and the remaining 25% to autumn crops [55]. Taking into account that Ence plans to process about 680 000 tons of biomass per year [23], the dryer could process 75% (510 000 tons) if it operates at its maximum capacity for about 3 400 h or, equivalently, 142 days (operating 24 h a day). For the rest of the year, it would operate at approximately one third of its maximum capacity to process the remaining biomass, leaving in that case 50 MW of thermal power available for the supply of the thermal network and being the annual average of the available power of 20.8 MW. Taking into account the above and the demand curve presented in Section 2.2.2 (Fig. 6), Eq. (2) expresses the availability of thermal power for the thermal network (Q_{net}) throughout the year considered hereinafter, so that the annual average power available for the network is about 20.1 MW (lower than the 20.8 MW that would be obtained at best).

Appendix B. Simplified calculation of a MST

To illustrate the process of obtaining a Minimum Spanning Tree (MST) from a set of selected points using the procedure described in Fig. 7 and Section 2.3, consider the graph shown in Fig. B.15(a). For the sake of simplicity, edge labels have been omitted, hence edges are referred to based on the nodes that they connect (for example, in the first row, the edges are denoted by $\overline{r_1 r_2}$ and $\overline{r_2 s_1}$). The following nomenclature is used for the nodes in the graph: yellow squares labeled s_i represent the selected points of supply in the graph (where $i \in \{1, \dots, 4\}$), and red circles labeled r_j represent simple nodes of the road network or non-selected points of supply (where $j \in \{1, \dots, 14\}$). Also, consider (only for this example) that the nodes represent geographical points, and due to their equidistance, all edges of the graph have a unit weight.

According to the above explanations, calculating the Minimum Spanning Tree (MST) of the graph involves determining the necessary edges to connect the nodes $s_1, s_2, s_3,$ and s_4 in such a way that the sum of weights of these edges is minimized. Since, in this case, the edges have a unit length, the objective is to connect these points with the minimum number of edges. To achieve this, the first step is to apply a Delaunay triangulation, which defines a new graph consisting only of the selected nodes and a new set of five edges (Fig. B.15(b)). This Delaunay triangulation ensures the connectivity of all nodes in a planar graph while maximizing the minimum angle of all triangles. In other words, it avoids forming triangles with very acute angles (as would occur if the edge $\overline{s_2 s_3}$ had been replaced by the edge $\overline{s_1 s_4}$). The goal is to generate only a few edges (instead of all possible combinations of the set of nodes $S = \{s_1, s_2, s_3, s_4\}$) between geographically close points to obtain a simpler graph (easier to compute).

In this article, the *delaunay* function from the MATLAB programming environment was used [56], to do so, employing the geographic

Table A.4
Nominal design data for Ence's plant.
Source: Retrieved from [23].

Source	Fagernäs et al. [54]	AAI. [23]
Technology	Band dryer	Band dryer
Biomass type	Sawdust, shavings and wood chips	Agricultural remains of greenhouse crops
Dry biomass outflow	8000–9000 kg/h	120 000 kg/h
Inlet moisture weight (52% average)	50%–60%	15%–80%
Exit moisture weight	10%–15%	<25%
Drying medium	Air or exhaust gases	Air
Evaporation capacity (H2O evaporated)	10 000 kg/h	–
Energy demand for evaporation (per kg of H2O evaporated)	4–5 MJ	–

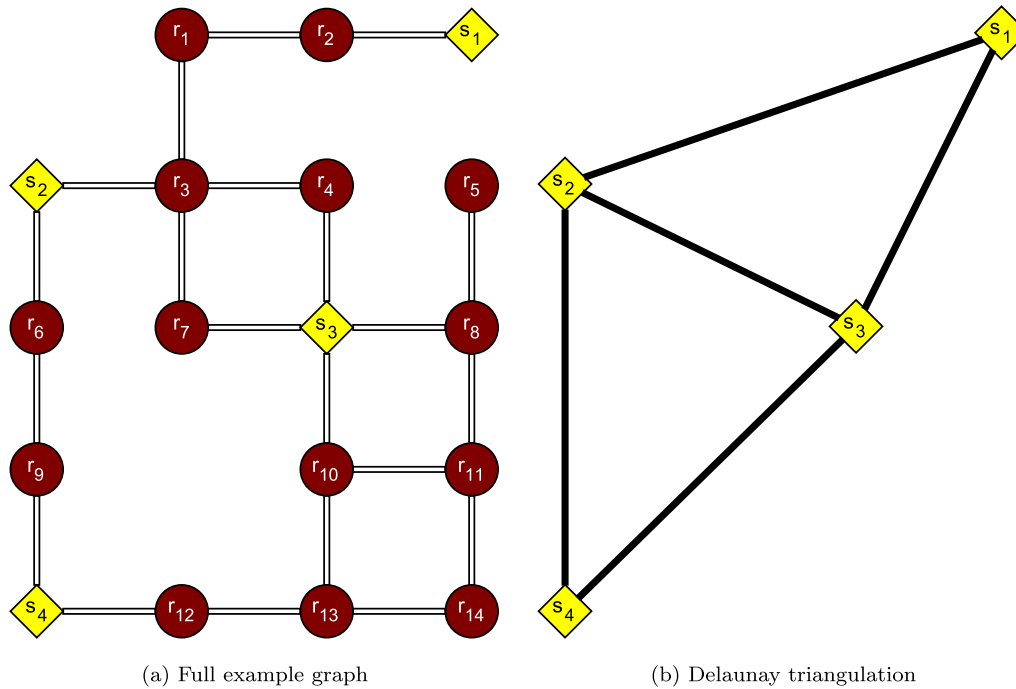


Fig. B.15. Example graph and Delaunay triangulation to calculate an MST.

coordinates imported from QGIS. A fundamental difference compared to other works in the literature is that the Delaunay triangulation is computed with points of supply, instead of using the centroids of the buildings or plots connected to the network [5,7]. The rationale behind this is that, since the pipes between the point of supply and the plot (sometimes referred to as the “secondary network”) are not considered part of the network, it does not make sense to use the centroids of each plot in this triangulation.

To assign weights to the new edges, it is necessary to analyze the original graph in Fig. B.15(a), as the geographical distance between nodes representing the edges in Fig. B.15(b) may not correspond to the road network that would be used to connect points of supply. To do this, pairs of points connected by the triangulation in Fig. B.15(b) are considered, and the minimum distance route that would connect them in the graph of Fig. B.15(a) is calculated through Dijkstra's algorithm. The choice of this algorithm over Johnson's algorithm, which is used by other authors [5,7], is due to the employment of the *shortestpath* function provided by the MATLAB programming environment with its default parameters [57]. This function is specifically designed for calculating paths but utilizes Dijkstra's algorithm for graphs with positive-weight edges.

In Fig. B.16(a), the result of the above operations on the original graph is depicted. Considering the edges defined in Figs. B.15(a) and B.15(b), and defining the function w as the one that returns the weight of a specific edge, the equivalences expressed in Eqs. (B.1) to (B.5) can be derived.

$$w(\overline{s_1s_2}) = w(\overline{s_1r_2}) + w(\overline{r_2r_1}) + w(\overline{r_1r_3}) + w(\overline{r_3s_2}) = 4 \tag{B.1}$$

$$w(\overline{s_1s_3}) = w(\overline{s_1r_2}) + w(\overline{r_2r_1}) + w(\overline{r_1r_3}) + w(\overline{r_3r_4}) + w(\overline{s_1r_4}) = 5 \tag{B.2}$$

$$w(\overline{s_2s_3}) = w(\overline{s_2r_3}) + w(\overline{r_3r_4}) + w(\overline{r_4s_3}) = w(\overline{s_2r_3}) + w(\overline{r_3r_7}) + w(\overline{r_7s_3}) = 3 \tag{B.3}$$

$$w(\overline{s_2s_4}) = w(\overline{s_2r_6}) + w(\overline{r_6r_9}) + w(\overline{r_9s_4}) = 3 \tag{B.4}$$

$$w(\overline{s_3s_4}) = w(\overline{s_3r_{10}}) + w(\overline{r_{10}r_{13}}) + w(\overline{r_{13}r_{12}}) + w(\overline{r_{12}s_4}) = 4 \tag{B.5}$$

The next step consists in obtaining the Minimum Spanning Tree (MST) of the graph defined in Fig. B.15(b) (with the already calculated weights of the five edges) by using Kruskal's algorithm. The MATLAB programming environment provides the *minspanntree* function [58], explicitly designed for this purpose. The choice of this algorithm over Prim's algorithm is because the degree of the graph defined in 2.2.1 corresponds to a rather sparse graph, not a dense one [59]. Once the spanning tree is obtained for the graph determined by the Delaunay triangulation, the equivalent tree with the nodes of the original graph is reconstructed, eliminating duplicated edges in the paths. In Fig. B.16(b), a possible result for the MST of the example graph is

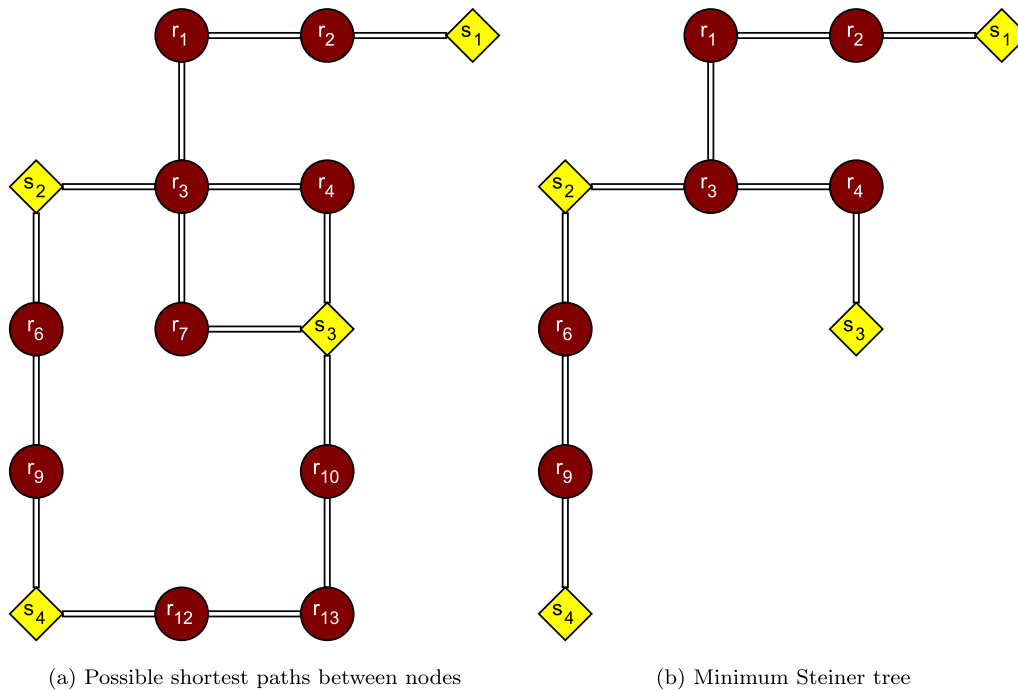


Fig. B.16. Application of the Dijkstra's and Kruskal's algorithms on the example graph.

shown, but note that the number of MSTs for a graph can be more than one and the described procedure does not ensure the convergence to an actual MST (the resulting graph could not satisfy the condition of having the minimum possible length).

References

[1] Bacquet A, Galindo Fernández M, Oger A, Themessl N, Fallahnejad M, Kranzl L, et al. Overview of markets and regulatory frameworks under the revised renewable energy directive. Tech. rep., Luxemburgo: Comisión Europea, Oficina de Publicaciones de la Unión Europea; 2021, <http://dx.doi.org/10.2833/962525>, <https://op.europa.eu/en/publication-detail/-/publication/5e1fd499-eabf-11ec-a534-01aa75ed71a1/language-en>. [Accessed 18 May 2023].

[2] Werner S. International review of district heating and cooling. Energy 2017;137:617–31. <http://dx.doi.org/10.1016/J.ENERGY.2017.04.045>.

[3] The Guardian. Eurozone inflation falls sharply as energy prices drop. 2023, [online] <https://www.theguardian.com/business/2023/mar/31/eurozone-inflation-falls-sharply-as-energy-prices-drop>. [Accessed 28 August 2023].

[4] Johansen K, Werner S. Something is sustainable in the state of Denmark: a review of the Danish district heating sector. Renew Sustain Energy Rev 2022;158:112117. <http://dx.doi.org/10.1016/J.RSER.2022.112117>.

[5] Lumberras M, Diarce G, Martín-Escudero K, Campos-Celador A, Larrinaga P. Design of district heating networks in built environments using GIS: A case study in Vitoria-Gasteiz, Spain. J Clean Prod 2022;349:131491. <http://dx.doi.org/10.1016/J.JCLEPRO.2022.131491>.

[6] QGISorg. QGIS Geographic Information System. QGIS Association. 2023, [online] <https://www.qgis.org>. [Accessed 18 May 2023].

[7] Unternährer J, Moret S, Joost S, Maréchal F. Spatial clustering for district heating integration in urban energy systems: Application to geothermal energy. Appl Energy 2017;190:749–63. <http://dx.doi.org/10.1016/J.APENERGY.2016.12.136>.

[8] Schmidt J, Stange P. Optimization of district heating network design. Energy Rep 2021;7:97–104. <http://dx.doi.org/10.1016/J.EGYR.2021.09.034>.

[9] Jebamalai JM, Marlein K, Laverge J, Vandeveld L, van den Broek M. An automated GIS-based planning and design tool for district heating: Scenarios for a Dutch city. Energy 2019;183:487–96. <http://dx.doi.org/10.1016/J.ENERGY.2019.06.111>.

[10] Boghetti R, Kämpf JH. Verification of an open-source Python library for the simulation of district heating networks with complex topologies. Energy 2024;290:130169. <http://dx.doi.org/10.1016/j.energy.2023.130169>.

[11] Pérez-Lombard L, Ortiz J, Pout C. A review on buildings energy consumption information. Energy Build 2008;40(3):394–8. <http://dx.doi.org/10.1016/J.ENBUILD.2007.03.007>.

[12] Gils HC, Cofala J, Wagner F, Schöpp W. GIS-based assessment of the district heating potential in the USA. Energy 2013;58:318–29. <http://dx.doi.org/10.1016/J.ENERGY.2013.06.028>.

[13] López JC, Baille A, Bonachela S, González-Real MM, Pérez-Parra J. Predicting the energy consumption of heated plastic greenhouses in South-Eastern Spain. Span J Agric Res 2006;4(4):289–96. <http://dx.doi.org/10.5424/SJAR/2006044-206>, [Accessed 18 May 2023].

[14] Valera DL, Belmonte LJ, Molina-Aiz FD, López A. Greenhouse agriculture in Almería: A comprehensive techno-economic analysis. Tech. rep., Almería: Publicaciones Cajamar; 2016, <https://publicacionescajamar.es/series-tematicas/economia/greenhouse-agriculture-in-almeria-a-comprehensive-techno-economic-analysis>. [Accessed 18 May 2023].

[15] Europa Press. Junta da autorización ambiental a Ence para la planta de cogeneración con biomasa de invernadero en El Ejido (Almería). 2022, [online] <https://www.europapress.es/andalucia/andalucia-verde-01334/noticia-junta-da-autorizacion-ambiental-ence-planta-cogeneracion-biomasa-invernadero-ejido-almeria-20221005144241.html>. [Accessed 18 May 2023].

[16] Wack Y, Serra S, Baelmans M, Reneaume J-M, Blommaert M. Nonlinear topology optimization of District Heating Networks: A benchmark of a mixed-integer and a density-based approach. Energy 2023;278:127977. <http://dx.doi.org/10.1016/j.energy.2023.127977>.

[17] Romero-Ramos JA, Gil JD, Cardemil JM, Escobar RA, Arias I, Pérez-García M. A GIS-AHP approach for determining the potential of solar energy to meet the thermal demand in southeastern Spain productive enclaves. Renew Sustain Energy Rev 2023;176:113205. <http://dx.doi.org/10.1016/j.rser.2023.113205>, [Accessed 18 May 2023].

[18] Otgonbayar T, Mazzotti M. Modeling and assessing the integration of CO2 capture in waste-to-energy plants delivering district heating. Energy 2024;290:130087. <http://dx.doi.org/10.1016/j.energy.2023.130087>.

[19] Cofely - Grupo GDF Suez. Guía integral de desarrollo de proyectos de redes de distrito de calor y frío. Tech. rep., Barcelona: Instituto Catalán de la Energía; 2012, https://www.adhac.es/portalsSrvcs/publicaciones/archivos/9_ADHAC-Guia-integral-de-desarrollo-de-proyectos-de-Redes-de-Distrito-de-Calor-y-Frio.pdf. [Accessed 18 May 2023].

[20] Salenbien R, Wack Y, Baelmans M, Blommaert M. Geographically informed automated non-linear topology optimization of district heating networks. Energy 2023;283:128898. <http://dx.doi.org/10.1016/j.energy.2023.128898>.

[21] Finkenrath M, Faber T, Behrens F, Leiprecht S. Holistic modelling and optimisation of thermal load forecasting, heat generation and plant dispatch for a district heating network. Energy 2022;250:123666. <http://dx.doi.org/10.1016/j.energy.2022.123666>.

[22] Oh S, Kim S-K. Impact of heat price regulation on the optimal district heating production mix and its policy implications. Energy 2022;239:122305. <http://dx.doi.org/10.1016/j.energy.2021.122305>.

[23] AAI/AL/142/22. Resolución del Delegado Territorial de Sostenibilidad, Medio Ambiente y Economía Azul en Almería, sobre la solicitud de Autorización Ambiental Integrada presentada por la empresa Ence Energía Este, S. L. U. para el "Proyecto de planta de cogeneración mediante restos vegetales procedentes de la agricultura intensiva" situada en el paraje Chozas

- de Redondo en el T. M. de El Ejido (Almería). Tech. rep., Consejería de Sostenibilidad, Medio Ambiente y Economía Azul de la Junta de Andalucía; 2022, <https://www.juntadeandalucia.es/medioambiente/servtc1/AAIo/iniVatAaioSearch.do>. [Accessed 18 May 2023].
- [24] Aalborg Energie Technik. AET biomass cogeneration plants. 2023, [online] <https://www.aet-biomass.com/en-GB/Home/Products/Biomass-Cogeneration-Plants.aspx>. [Accessed 18 May 2023].
- [25] IEA. Technology roadmap: Bioenergy for heat and power. Tech. rep., International Energy Agency; 2012, https://www.globalbioenergy.org/uploads/media/1205 IEA_-_Technology_Roadmap_Bioenergy_for_Heat_and_Power.pdf. [Accessed 18 May 2023].
- [26] Ministerio de Agricultura. Servicio ATOM de descarga de datos SIGPAC. Tech. rep., 2022, https://www.fega.gob.es/orig/pdfs/202201_Informacion_servicio_descargas_SIGPAC.pdf. [Accessed 18 May 2023].
- [27] IDAE. Ahorro y eficiencia energética en invernaderos. Tech. rep., Madrid: Instituto para la Diversificación y Ahorro de la Energía; 2008, <https://www.idae.es/publicaciones/ahorro-y-eficiencia-energetica-en-invernaderos>. [Accessed 18 May 2023].
- [28] Rodríguez F, Berenguel M, Guzmán JL, Ramírez-Arias A. Modeling and control of greenhouse crop growth. Springer; 2015, <http://dx.doi.org/10.1007/978-3-319-11134-6>, <http://link.springer.com/10.1007/978-3-319-11134-6>. [Accessed 18 May 2023].
- [29] Morales A. Cómo descargar las parcelas del SIGPAC y visualizarlas en QGIS. 2020, MappingGIS [online] <https://mappinggis.com/2020/03/como-descargar-las-parcelas-del-sigpac-en-qgis-el-caso-de-castilla-y-leon/>. [Accessed 18 May 2023].
- [30] IGN. Geoportal oficial del Instituto Geográfico Nacional de España. 2023, [online] <http://www.ign.es>. [Accessed 18 May 2023].
- [31] Lantmateriet. ETRS89. 2023, [online] <https://www.lantmateriet.se/en/geodata/gps-geodesi-och-swepos/reference-systems/three-dimensional-systems/etrs89/>. [Accessed 26 August 2023].
- [32] Berge C. The theory of graphs. Mineola, Nueva York: Dover Publications, Inc.; 2001.
- [33] Palmier P. Networks — QGIS Python plugins repository. 2022, [online] <https://plugins.qgis.org/plugins/networks/>. [Accessed 18 May 2023].
- [34] The MathWorks Inc. Find minimum of function using genetic algorithm - MATLAB ga. 2023, [online] <https://es.mathworks.com/help/gads/ga.html>. [Accessed 18 May 2023].
- [35] Klokant Technologies GmbH. EPSG:7030. 2022, [online] <https://epsg.io/7030-ellipsoid>. [Accessed 18 May 2023].
- [36] JRC. PVGIS user manual. 2022, Centro Común de Investigación. Comisión Europea [online] https://joint-research-centre.ec.europa.eu/pvgis-online-tool/getting-started-pvgis/pvgis-user-manual_en. [Accessed 18 May 2023].
- [37] Huld T, Müller R, Gambardella A. A new solar radiation database for estimating PV performance in Europe and Africa. Sol Energy 2012;86(6):1803–15. <http://dx.doi.org/10.1016/j.solener.2012.03.006>, [Accessed 18 May 2023].
- [38] Garzoli KV, Blackwell J. An analysis of the nocturnal heat loss from a double skin plastic greenhouse. J Agric Eng Res 1987;36(2):75–86. [http://dx.doi.org/10.1016/0021-8634\(87\)90114-4](http://dx.doi.org/10.1016/0021-8634(87)90114-4), [Accessed 18 May 2023].
- [39] Liu Y, Tang H, Chen Y, Wang D, Song C. Optimization of layout and diameter for distributed solar heating network with multi-source and multi-sink. Energy 2022;258:124788. <http://dx.doi.org/10.1016/j.energy.2022.124788>.
- [40] Merlet Y, Baviere R, Vasset N. Formulation and assessment of multi-objective optimal sizing of district heating network. Energy 2022;252:123997. <http://dx.doi.org/10.1016/j.energy.2022.123997>.
- [41] Byrka J, Grandoni F, Rothvoß T, Sanità L. An improved LP-based approximation for steiner tree. In: Proceedings of the forty-second ACM symposium on theory of computing. STOC '10, Nueva York, Estados Unidos: Association for Computing Machinery; 2010, p. 583–92. <http://dx.doi.org/10.1145/1806689.1806769>, [Accessed 18 May 2023].
- [42] Fernando J. Net Present Value (NPV): What it means and steps to calculate it. 2023, Investopedia [online] <https://www.investopedia.com/terms/n/npv.asp>. [Accessed 25 August 2023].
- [43] Hayes A. Cost of capital: what it is, why it matters, formula, and example. 2022, Investopedia [online] <https://www.investopedia.com/terms/c/costofcapital.asp>. [Accessed 18 May 2023].
- [44] Vega A, Yarahmadi N, Jakubowicz I. Determining the useful life of district heating pipes: Correlation between natural and accelerated ageing. Polym Degrad Stab 2020;175:109117. <http://dx.doi.org/10.1016/j.polymdegradstab.2020.109117>, [Accessed 18 May 2023].
- [45] Nussbaumer T, Thalmann S. Influence of system design on heat distribution costs in district heating. Energy 2016;101:496–505. <http://dx.doi.org/10.1016/j.energy.2016.02.062>, [Accessed 18 May 2023].
- [46] Persson U, Werner S. Heat distribution and the future competitiveness of district heating. Appl Energy 2011;88(3):568–76. <http://dx.doi.org/10.1016/j.apenergy.2010.09.020>, [Accessed 18 May 2023].
- [47] Persson U, Möller B, Sánchez-García L, Wiechers E. District heating investment costs and allocation of local resources for EU28 in 2030 and 2050. Tech. rep., Zenodo; 2021, <http://dx.doi.org/10.5281/ZENODO.4892271>, [Accessed 18 May 2023].
- [48] Soltero VM, Quirosa G, Rodríguez D, Peralta ME, Ortiz C, Chacartegui R. A profitability index for rural biomass district heating systems evaluation. Energy 2023;282:128395. <http://dx.doi.org/10.1016/j.energy.2023.128395>.
- [49] Gudmundsson O, Thorsen JE, Zhang L. Cost analysis of district heating compared to its competing technologies. WIT Trans Ecol Environ 2013;176:3–13.
- [50] Danish Energy Agency. Technology data for heating installations. Tech. rep., 2016, https://ens.dk/sites/ens.dk/files/Analyser/technology_data_catalogue_for_individual_heating_installations.pdf. [Accessed 18 May 2023].
- [51] Nussbaumer T, Thalmann S. Status report on district heating systems in IEA countries. Tech. rep., Verenum, Zürich, Suiza: International Energy Agency; 2014, https://task32.ieabioenergy.com/wp-content/uploads/sites/2/2017/03/wp_2_Task32_DHS_Status_Report.pdf. [Accessed 18 May 2023].
- [52] OMIE. Day ahead minimum, average and maximum price. 2023, [online] <https://www.omie.es/en/market-results/interannual/daily-market/daily-prices?scope=interannual>. [Accessed 18 May 2023].
- [53] Sean R. When is inflation good for the economy? 2023, Investopedia [online] <https://www.investopedia.com/ask/answers/111414/how-can-inflation-be-good-economy.asp>. [Accessed 18 May 2023].
- [54] Fagnäs L, Brammer J, Wilén C, Lauer M, Verhoeff F. Drying of biomass for second generation synfuel production. Biomass Bioenergy 2010;34(9):1267–77. <http://dx.doi.org/10.1016/j.biombioe.2010.04.005>, [Accessed 18 May 2023].
- [55] Duque-Acevedo M, Belmonte-Ureña LJ, Plaza-Úbeda JA, Camacho-Ferre F. The management of agricultural waste biomass in the framework of circular economy and bioeconomy: An opportunity for greenhouse agriculture in Southeast Spain. Agronomy 2020;10(4). <http://dx.doi.org/10.3390/agronomy10040489>, [Accessed 18 May 2023].
- [56] The MathWorks Inc. Delaunay triangulation - MATLAB delaunay. 2023, [online] <https://es.mathworks.com/help/matlab/ref/delaunay.html>. [Accessed 18 May 2023].
- [57] The MathWorks Inc. Shortest path between two single nodes - MATLAB shortestpath. 2023, [online] <https://es.mathworks.com/help/matlab/ref/graph.shortestpath.html#buofmw7-1-Method>. [Accessed 18 May 2023].
- [58] The MathWorks Inc. Minimum spanning tree of graph - MATLAB minspantree. 2023, [online] <https://es.mathworks.com/help/matlab/ref/graph.minspantree.html>. [Accessed 18 May 2023].
- [59] argha_c14. Difference between Prim's and Kruskal's algorithm for MST. 2019, GeeksforGeeks [online] <https://www.geeksforgeeks.org/difference-between-prim-and-kruskals-algorithm-for-mst/>. [Accessed 18 May 2023].